The Petrology and Geochemistry of the 2021 Fagradalsfjall Eruption, Iceland

E W Marshall, A Caracciolo, E Bali, S A Halldórsson, S Matthews, E Ranta, M B Rasmussen, J G Robin, G H Guðfinnson, J Maclennan, et al.

AGU ADVANCING EARTH AND SPACE SCIENCES

AGU Advances

RESEARCH ARTICLE
10.1029/2024AV001310

The Petrology and Geochemistry of the 2021 Fagradalsfjall Eruption, Iceland: An Eruption Sourced From Multiple, Compositionally Diverse, Near-Moho Sills

E. W. Marshall[1,2], A. Caracciolo[1], E. Bali[1], S. A. Halldórsson[1], S. Matthews[1], E. Ranta[3], M. B. Rasmussen[4], J. G. Robin[1], G. H. Guðfinnson[1], J. Maclennan[5], C. Bosq[6], D. Auclair[6], O. Sigmarsson[1,6], H. Merrill[1], B. Gísladóttir[1], S. Johnson[1], N. Löw[1], A. Stracke[7], and F. Genske[7]

[1]Nordic Volcanological Center, Institute of Earth Sciences, University of Iceland, Reykjavík, Iceland, [2]GeoZentrum Nordbayern, Friedrich-Alexander-Universität Erlangen-Nürnberg, Erlangen, Germany, [3]Department of Geosciences and Geography, University of Helsinki, Helsinki, Finland, [4]Department of Geosciences and Natural Resource Management, University of Copenhagen, Copenhagen, Denmark, [5]Department of Earth Sciences, University of Cambridge, Cambridge, UK, [6]Laboratoire Magmas et Volcans, CNRS - Université Clermont Auvergne, Aubière, France, [7]Institut für Mineralogie, Universität Münster, Münster, Germany

Peer Review The peer review history for this article is available as a PDF in the Supporting Information.

Key Points:

- We use high frequency sampling to observe rapid changes in lava composition during the 183 day 2021 Fagradalsfjall eruption
- The eruption was sourced from 12 to 15 km depth, corresponding to the lowermost crust and the crust-mantle boundary
- Lavas show broad compositional variability over short time periods, requiring input from multiple compositionally distinct magma bodies

Supporting Information:

Supporting Information may be found in the online version of this article.

Correspondence to:

E. W. Marshall,
edmarshall@hi.is

Citation:

Marshall, E. W., Caracciolo, A., Bali, E., Halldórsson, S. A., Matthews, S., Ranta, E., et al. (2024). The petrology and geochemistry of the 2021 Fagradalsfjall eruption, Iceland: An eruption sourced from multiple, compositionally diverse, near-Moho sills. *AGU Advances*, *5*, e2024AV001310. https://doi.org/10.1029/2024AV001310

Received 10 MAY 2024
Accepted 27 SEP 2024

Author Contributions:

Conceptualization: E. W. Marshall, A. Caracciolo, E. Bali, S. A. Halldórsson, M. B. Rasmussen, J. Maclennan
Data curation: E. W. Marshall, O. Sigmarsson
Formal analysis: E. W. Marshall, A. Caracciolo, E. Bali, S. A. Halldórsson, S. Matthews, E. Ranta, J. Maclennan, O. Sigmarsson, A. Stracke
Funding acquisition: E. W. Marshall, E. Bali, S. A. Halldórsson

Abstract

Magmatic processes at the crust-mantle boundary (i.e., Moho) are commonly studied *post facto* at fossil ophiolites, oceanic core complexes, or inferred from the compositions of crystals or melt inclusions. The 2021 eruption at Fagradalsfjall on the Reykjanes Peninsula, Iceland, was supplied from magma bodies near the Moho and offers a unique opportunity to study the timescales, structure, and syn-eruptive processes of near-Moho magmatic systems at ∼15 km depth. Here, we present a comprehensive petrological and geochemical investigation of the full 183 day eruption that is based on frequent sampling of the eruption. Lavas erupted in the first 45 days displayed significant and sudden changes in geochemistry, followed by lower amplitude fluctuations until the end of the eruption. This variability can be explained by contribution from multiple magma bodies, as best distinguished using Sr-Nd-Hf-Pb isotope systematics. The lavas display unusual trace element and radiogenic isotope compositions compared to other Icelandic basalts, but are similar to other rare, highly incompatible element enriched lavas on the Reykjanes Peninsula, and thus these lavas may represent a distinct suite of Reykjanes Peninsula basalts. Our geochemical and petrological observations show that numerous, compositionally variable bodies of magma must exist in the lowermost crust or at the crust-mantle boundary. These near-Moho magma bodies transfer magma between one another on timescales as short as days-to-months, but partially crystallize over longer time periods, and periodically inject into the overlying crust.

Plain Language Summary

The 2021 Fagradalsfjall eruption is the first on Iceland's Reykjanes Peninsula in ∼800 years and likely is the harbinger of a renewed period of volcanism on the peninsula, as evidenced by subsequent eruptions at Fagradalsfjall and Svartsengi. For evaluating the potential hazard of the new eruptive period, we must understand how these new volcanic systems work. Here, we investigate the chemical and mineralogical properties of the 2021 Fagradalsfjall lava in order to identify the structure, igneous processes, and origins of the magmas feeding the new eruptions. We find that the 2021 eruption lavas have highly unusual compositions compared to most Icelandic basaltic eruptions and are sourced deeper, from magma bodies at the bottom of the crust. In contrast to the rather homogeneous chemical compositions of most basaltic eruptions, the compositions of the 2021 Fagradalsfjall lavas are extremely variable. This is explained by the lava being fed from multiple independent magma bodies close to the crust-mantle boundary. The 2021 Fagradalsfjall eruption is the first that allows direct investigation of a "living" magma system hosted near the crust-mantle boundary. The Fagradalsfjall deep magma system is characterized by many, compositionally diverse, magma bodies that exchange magma with one another on days-to-weeks timescales and occasionally intrude into the overlying crust.

1. Introduction

The 2021 eruption within the Fagradalsfjall volcanic system marked the first eruption on the Reykjanes Peninsula in ∼800 years, and the first eruption at Fagradalsfjall in >2,400 years (Sæmundsson et al., 2016). Detailed studies of the eruptive history of the Reykjanes Peninsula suggest that volcanism occurs in cycles, with periods of

Investigation: E. W. Marshall, A. Caracciolo, E. Bali, S. A. Halldórsson, S. Matthews, M. B. Rasmussen, J. G. Robin, G. H. Guðfinnson, C. Bosq, D. Auclair, O. Sigmarsson, H. Merrill, B. Gísladóttir, S. Johnson, N. Löw, A. Stracke, F. Genske
Methodology: E. W. Marshall, A. Caracciolo, E. Bali, S. A. Halldórsson, M. B. Rasmussen, O. Sigmarsson, A. Stracke
Project administration: E. W. Marshall, E. Bali, S. A. Halldórsson
Resources: E. W. Marshall, A. Caracciolo, E. Bali, S. A. Halldórsson, S. Matthews, E. Ranta, M. B. Rasmussen, O. Sigmarsson, S. Johnson
Supervision: E. W. Marshall, A. Caracciolo, O. Sigmarsson
Visualization: E. W. Marshall, A. Caracciolo
Writing – original draft: E. W. Marshall, A. Caracciolo, E. Bali
Writing – review & editing: E. W. Marshall, A. Caracciolo, E. Bali, S. A. Halldórsson, S. Matthews, E. Ranta, M. B. Rasmussen, J. G. Robin, G. H. Guðfinnson, J. Maclennan, C. Bosq, D. Auclair, O. Sigmarsson, H. Merrill, B. Gísladóttir, N. Löw, A. Stracke, F. Genske

volcanic activity across the peninsula lasting a few hundred years, and an entire cycle lasting approximately 1,200 years (Sæmundsson et al., 2020). The 2021 Fagradalsfjall eruption may therefore represent the first eruption in a renewed cycle of Reykjanes Peninsula volcanism that may last centuries. Subsequent eruptions have followed the 2021 eruption within both the Fagradalsfjall and Svartsengi volcanic systems, illustrating the continuation of volcanic activity on the peninsula. Given that the majority of Iceland's population lives on the Reykjanes Peninsula, a clear understanding of these early eruptions is essential for hazard management and eruption forecasting along the peninsula.

The 2021 eruption at Fagradalsfjall differs markedly from most Icelandic basaltic eruptions (Halldórsson et al., 2022), which are typically sourced from mid-crustal reservoirs (Baxter et al., 2023; Caracciolo et al., 2020, 2023; Halldórsson et al., 2018; Neave & Putirka, 2017). The 2021 Fagradalsfjall eruption was sourced deeper-from depths close to the crust-mantle boundary (or "Moho"; Halldórsson et al., 2022). Furthermore, basaltic eruptions in Iceland are usually homogenous in terms of geochemical mantle source tracers (e.g., 1783–1784 Laki, 2014–2015 Holuhraun; Halldórsson et al., 2018; Sigmarsson et al., 1991), but the 2021 eruption was highly variable. It displayed several times more mantle-derived variability than the combined variability of all lavas from the ∼800–1240 CE cycle of volcanism on the Reykjanes Peninsula (hereafter referred to as the "800–1240 CE Fires"), and more than any well-characterized individual lava unit known globally (Halldórsson et al., 2022). Finally, basaltic eruptions typically decline exponentially in lava effusion rate over time, but the effusion rate of the 2021 eruption stayed remarkably constant and even increased over the course of the eruption (Pedersen et al., 2022). These remarkable features show that the magmatic system of Fagradalsfjall represents an unusual case of basaltic volcanism.

The deep sourcing of the eruption presents an additional opportunity to study basalts from the deepest levels of a crustal basaltic magmatic system. Deep basaltic magmatic systems have been studied extensively *post facto* at ophiolites and oceanic core complexes, or via xenoliths, lava crystal cargoes, or melt inclusions (e.g., Kelemen et al., 1997; Koga et al., 2001; Lambart et al., 2019; Maclennan et al., 2003; Mutch, Maclennan, Holland, & Buisman, 2019). Hence, the 2021 Fagradalsfjall eruption presents a new opportunity to study active near-Moho basaltic magmatic systems through high frequency sampling of its lavas. As these deep magma plumbing systems play a key role in the accretion and construction of the lower crust, as well as feeding shallower magma chambers, better understanding of these deep systems is fundamental. The image of deep basaltic magmatic systems, as drawn from past studies, is that chemically heterogeneous, near-primary basaltic magmas accumulate at or near the crust-mantle boundary, where they mix, reside, and partially crystallize, before intermittent injection into the overlying crust (Kelemen & Aharonov, 1998; Kelemen et al., 1997; Korenaga & Kelemen, 1997; Maclennan, 2019). High-frequency sampling of the 2021 Fagradalsfjall eruption allows evaluation of this hypothesis, along with added details from an active near-Moho magma system.

The significant lava compositional variation and the unusual change in effusion rate over time in the 2021 Fagradalsfjall eruption are atypical features for an eruption fed from a single well-mixed magma reservoir (Halldórsson et al., 2022; Pedersen et al., 2022). Previously investigated eruptions along the East Pacific Rise showed variable lava compositions within single basalt lava units and such variations were attributed to active mixing within a heterogeneous axial magma chamber during eruption (Bergmanis et al., 2007). However, it is also possible that the 2021 eruption is fed from multiple magma chambers. Multiple connected magma bodies in the deep crust have been suggested from ground deformation studies of Afar, East Africa (La Rosa et al., 2024). Similarly, anomalously long deflation at the summit of Kilauea, and prolonged lava effusion during the 2018 eruption is consistent with sourcing from multiple magma reservoirs (Townsend & Huang, 2022). The 1975–1984 Krafla eruption in Iceland showed diverse lava compositional variations that may reflect sourcing from multiple magma reservoirs in the upper and lower crust (Rooyakkers et al., 2024). Finally, compositional variations along eruptive fissures in the 2024 Svartsengi eruptions reveal that the source of the erupted lavas is a complex of multiple mid-crustal reservoirs (Matthews et al., 2024). Therefore, multiple magma reservoirs may also feed the 2021 Fagradalsfjall eruption.

Here, we investigate the petrology and geochemistry of the entire 2021 Fagradalsfjall eruption to better understand the structure, processes, and mantle sources of its deep volcanic system. This study builds, and expands, upon the prior work by Halldórsson et al. (2022), which focused on the first 50 days of the 183 day eruption. In comparison to Halldórsson et al. (2022), this study contains 26 additional samples, spanning the whole duration of the eruption, and includes new major element analyses of glass and mineral phases as well as new trace element

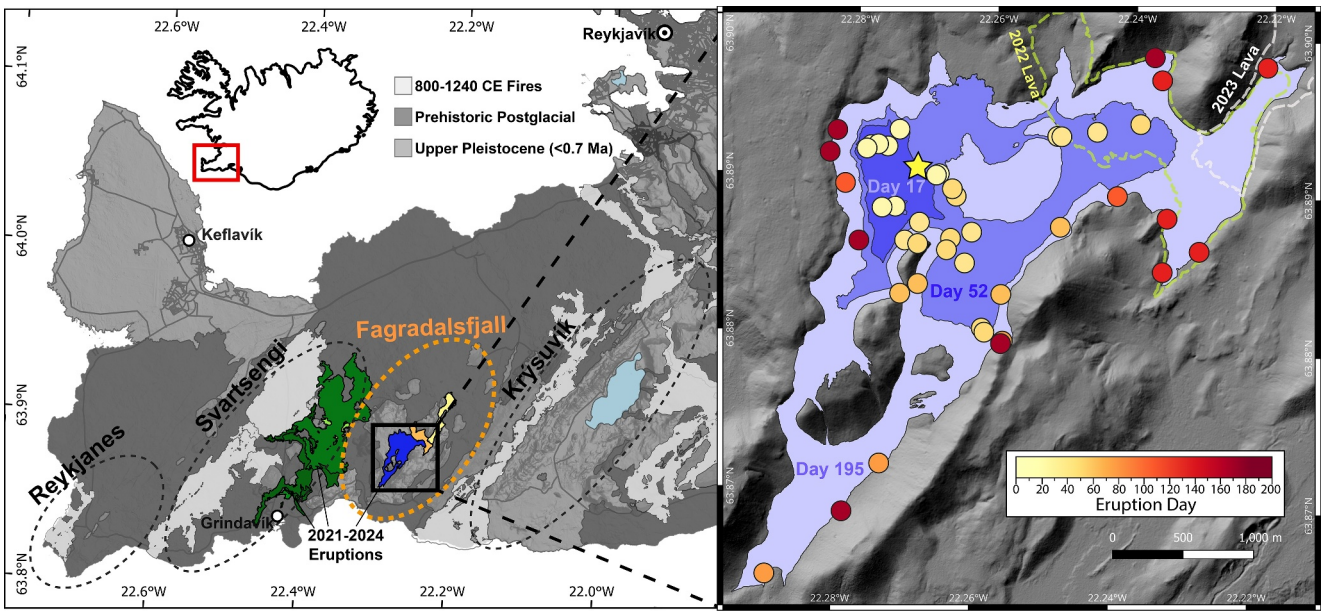

Figure 1. Regional and sample locality map of the 2021 Fagradalsfjall eruption. Top left: outline of Iceland with Reykjanes Peninsula shown with a red box. Left: Map of Reykjanes Peninsula. Areas of pre-2021 lavas are mapped in gray, see legend (Sæmundsson et al., 2016). The extents of lavas from the 2021–2024 eruptions are shown in color (Gunnarson et al., 2023; Umbrotasjá, Landmaelingar). The 2021 lava field is shown in blue. Dashed ovals highlight the locations of the Reykjanes, Svartsengi, Fagradalsfjall, and Krýsuvík volcanic systems (Sæmundsson et al., 2020). Right: Sample locality map of the 2021 Fagradalsfjall lava field. Samples are shown as circles, whose color corresponds to eruption date as given in the color bar. The changing shape of the lava field throughout the eruption is shown by the three fields labeled days 17, 52, and 195, which correspond to the days at which the lava outline was obtained, note that the eruption is 183 days long (Pedersen et al., 2022). The outlines of the lava fields produced by the 2022 (yellow) and 2023 (white) Fagradalsfjall eruptions are shown in dashed outline. The yellow star represents the location of the central vent after eruption day 39.

and Sr-Nd-Hf-Pb radiogenic isotope analyses of both the samples featured in Halldórsson et al. (2022) and the 26 new samples (see Table S1 in Supporting Information S2). We find that the significant and sudden changes in trace element and radiogenic isotope ratios of erupted lavas are related to a complex magmatic reservoir structure, wherein magma is stored in multiple bodies at near-Moho depths and the compositional variability of the erupted lavas reflects compositional differences between magma bodies. A complex, multi-bodied reservoir structure, and erosion of crystal mush around the eruptive conduit, likely explains the prolonged, low, and relatively constant effusion rate of the eruption. Our study depicts a near-Moho region containing multiple, coexisting basaltic magma bodies with distinct and unusual geochemical compositions. We show that magmas from different magma bodies mix at depth and subsequently erupt on day-to-weeks timescales. Although a seemingly rare phenomenon, our results show that dikes emanating from near-Moho magma bodies can traverse the entire crust, erupting directly onto the surface.

2. Geological Background

The 2021 Fagradalsfjall eruption occurred in southwest Iceland on the Reykjanes Peninsula (Figure 1). As a part of the Icelandic rift, the Reykjanes Peninsula represents an on-land extension of the mid-Atlantic Ridge that is fed by the upwelling Icelandic plume (Peate et al., 2009). The Reykjanes Peninsula has highly oblique spreading, inclined by about 55° from perpendicular spreading (Einarsson et al., 2023). The Reykjanes Peninsula can be divided into several volcanic systems that form a series of linear, en enchelon volcanic systems (see Sæmundsson & Sigurgeirsson, 2013). From west to east, these volcanic systems are: Reykjanes, Svartsengi, Fagradalsfjall, Krýsuvík, Brennisteinsfjöll, and Hengill. Except for Hengill, none of these volcanic systems contain a central volcano and have only produced basaltic and picritic lavas (Sæmundsson & Sigurgeirsson, 2013). Unlike the other Reykjanes Peninsula volcanic systems, the Fagradalsfjall volcanic system does not have a fissure swarm and has experienced little postglacial volcanism (Sæmundsson & Sigurgeirsson, 2013). The Fagradalsfjall volcanic system comprises a small (~6 km wide) complex of tuyas, hyaloclastite mounds and ridges, and postglacial lavas (Figure 1). To clarify, although in this publication we use "Fagradalsfjall" to refer to

the volcanic system as a whole, "Fagradalsfjall" is also the name of the largest tuya within the eponymous Fagradalsfjall volcanic system.

Volcanism on the Reykjanes Peninsula occurs in cyclic episodes of fissure eruptions with a period of every ∼1,200 years with each volcanic episode lasting ∼500 years and a ∼700 year period of quiescence between episodes (Sæmundsson et al., 2020). The previous episode of eruptions on the Reykjanes Peninsula occurred between ∼800 CE and 1240 CE, overlapping with the settlement of Iceland (i.e., the 800–1240 CE Fires), but two older cycles at 2,500–2,000 years ago, and 3,500–3,000 years ago are also known (Sæmundsson & Sigurgeirsson, 2013). In each of the three previous eruption episodes there were eruptions at the Reykjanes, Svartsengi, Krýsuvík, and Brennistensfjöll volcanic systems. No eruptions at Fagradalsfjall have occurred in >2,400 years (Sæmundsson et al., 2016).

Recent magmatic unrest on the Reykjanes Peninsula began with a seismic swarm just south of Fagradalsfjall in mid-December 2019 (Greenfield et al., 2022; Sigmundsson et al., 2022). Another swarm east of Svartsengi on 20 February 2020, preceded repeated cycles of inflation and deflation at that location until July 2020 (Cubuk-Sabuncu et al., 2021; Flóvenz et al., 2022). On 24 February 2021, a M_w 5.64 earthquake initiated an unprecedently intense seismic swarm at Fagradalsfjall (Sigmundsson et al., 2022). The seismicity coincided with ground deformation that indicated the injection of a NE-SW striking dike at Fagradalsfjall. Seismicity and ground deformation continued until about 16 March, when there was a decline in the observed ground deformation rate and seismicity (Sigmundsson et al., 2022). The eruption began in the evening of 19 March 2021 with a 180 m-long fissure in the Geldingadalir area of Fagradalsfjall effusing basaltic lavas (Pedersen et al., 2022).

Although the effusion rate of most basaltic eruptions in Iceland declines over time (Gudmundsson et al., 2016; Pedersen et al., 2022), that of the 2021 Fagradalsfjall eruption did not, and rather displayed a complex relationship between effusion rate, eruptive style, and time (a brief summary is given here, see Pedersen et al., 2022). The eruption began on 19 March 2021 at low time-averaged effusion rates (1–8 m^3/s) with continuous effusion from one vent. On 5 April, additional vents opened with no change in effusion rate. These additional vents would steadily become inactive over the following weeks. On April 27th, with effusion occurring at only one vent, continuous lava fountaining suddenly began, with periodic fountains beginning on May 2nd (Eibl et al., 2023; Scott et al., 2023), coinciding with an increase in time-averaged effusion rate to ∼13 m^3/s. Until the end of the eruption, time averaged effusion rate stayed over 8 m^3/s and was focused on a single eruptive vent (Figure 1).

3. Sampling

Freshly erupted materials were frequently (approximately weekly, longest gap is 16 days) sampled as part of the petrological monitoring of the eruption. Three types of samples were obtained: quenched lava (i.e., by scooping molten lava into a water-filled bucket), naturally cooled lava, and air-quenched tephra. Sampling was conducted so that each sample had clear field context. Naturally cooled and water-quenched lava samples were collected only from flows where the field context was unambiguously clear (i.e., known time of flow emplacement and known duration of residency on the lava on the lava field), as observed in the field or recorded on the webcam network of the Icelandic Meteorological Office. Tephra samples were collected from the ground (or, in one case caught mid-air) when they could be connected to a particular tephra fall event or period. The collection of glassy materials was prioritized: glassy tephra or vent splatter, glassy pahoehoe flowtops, and quenched lavas. A total of 51 samples are presented in this work, 25 of which were originally described in Halldórsson et al. (2022), see Table S1 in Supporting Information S2 for sample information.

The "eruption date," or the inferred date of eruption from the vent, was estimated for each sample. The eruption date could be estimated very precisely when a particular lava flow was directly seen emerging from the vent before emplacement and sampling. However, the eruption dates for other samples could not be so precisely determined. In these cases, a range of dates that encompasses the possible eruption dates was assigned to the sample, never higher than nine possible days. Lava units whose eruption dates were difficult to constrain were avoided entirely. For many samples, the eruption date and the sampling date are not the same, because sometimes the lavas were sampled more than a week following emplacement. These efforts resulted in a data set where the timing of each sample is well defined, permitting the construction of a high-quality time series.

4. Methods

4.1. Analytical Methods

Most analytical methods followed procedures identical to those used by Halldórsson et al. (2022), who analyzed samples from the first 40 days of the 2021 Fagradalsfjall eruption, and the differences in methods are detailed below. All data, including standard data, are reported in Tables S2–S10 in Supporting Information S2. The methods for determining trace element concentrations were changed slightly from those used in Halldórsson et al. (2022) and some samples were remeasured using updated methods in order to maintain consistent analytical procedures across the eruption and to add additional elements. This study focuses on four different types of samples: glass, minerals, whole rock, and macrocryst-free matrix. Glass and minerals were hand-picked from fragments of tephra or lava and analyzed via in situ electron microprobe analysis. Whole rock samples represent hand-picked, clean coarse lava pieces. Macrocryst-free matrix samples were prepared by hand picking macrocryst-free fragments of lava matrix from crushed coarse (<1 mm) lava pieces under a stereo microscope.

Major element concentrations of picked glasses and minerals were determined on an JEOL JXA-8320 SuperProbe electron microprobe at the University of Iceland. For details on the electron microprobe settings and methods for all analyzed phases, see Halldórsson et al. (2022). Precision for glass analyses, as measured by replicate analyses of basalt glass reference material A99, are less than 2% (2 SD) for elements with abundances greater than 10 wt%, less than 3% for TiO_2, MgO, and CaO, less than 7.5% for Na_2O and K_2O, and less than 30% for MnO, SO_3, and Cl, see Tables S6–S10 in Supporting Information S2.

Major element concentrations of whole rock lava and macrocryst-free matrix were determined via Inductively Coupled Plasma Optical Emission Spectroscopy (ICP-OES) on a Thermo iCap 7400 Duo at the University of Iceland. Procedures for whole rock powder digestion and ICP-OES analysis are identical to those of Halldórsson et al. (2022). Whole rock samples were ground in a tungsten carbide disc mill. For major element analysis of macrocryst-free matrix, 1 g of macrocryst-free matrix was hand-picked and ground in an agate mortar and pestle with a small amount of 18 MΩ water added. The water-powder slurry was dried in a clean plastic vial to produce a dry powder. The macrocryst-free matrix powder was then analyzed in the same manner as whole rock powders. Based on replicates of basaltic reference materials BHVO-1, W-2, and BIR-1, precisions for all elements were less than 5% (2 SD; and often less than 2%), see Table S2 in Supporting Information S2.

Trace element concentrations of lavas were determined via solution Inductively Coupled Plasma Quadrupole Mass Spectrometry (ICP-Q-MS) using a Thermo iCap RQ ICP-MS at the University of Iceland. Sample dissolution procedures were performed in a metal-free clean laboratory. Hand-picked pieces of macrocryst-free matrix were rinsed in 18.2 MΩ water, boiled in 18.2 MΩ water, and rinsed again to remove dust and soluble surficial contaminants. About 30–50 mg of the cleaned glass fragments were then weighed and loaded into 7 ml Savillex Teflon vials. They were then digested in a HF-HNO_3 solution. Insoluble fluorides were removed by repeated dissolution and dry down steps using solutions of concentrated HNO_3 and HNO_3-HCl. Once complete dissolution was ensured, the samples were dissolved in a mixture of HNO_3 and HCl and the mixture was decanted into an acid-cleaned HDPE bottle containing 18.2 MΩ water, to make a 2% HNO_3 + 0.5% HCl analysis solution with a dilution factor of ∼5,000. The larger digestion volume, combined with the addition of HCl, improved the reproducibility of HFSE concentration analysis. Samples analyzed by Halldórsson et al. (2022) were remeasured using the method here in order to have consistent methodology and permit the analysis of Nb and Ta. The new procedure had no effect on non-HFSE lithophile elements (e.g., Ba, U, Th, REEs), and therefore the new set of analyses represent a duplicate set for those elements and samples. Based on the reproducibility of reference material W-2 and the duplicates, analytical uncertainties were less than 5% for most elements, See Table S4 in Supporting Information S2.

Measurements of Sr and Nd radiogenic isotope ratios were performed at Laboratoire Magmas et Volcans at Université Clermont Auvergne using a Thermo Triton thermal ionization mass spectrometer. Analytical methods followed those described in Halldórsson et al. (2022). Sr and Nd isotope analysis of reference material AGV-1 corresponds, within uncertainty, to the average values presented in Weis et al. (2006), see Table S5 in Supporting Information S2.

Measurements of Pb isotope ratios were performed at both University of Iceland and at University of Münster on a Nu Plasma 1 and Thermo Neptune *Plus*, respectively. Measurements of Hf isotope ratios were performed entirely at University of Münster on a Thermo Neptune *Plus*. All chemical separations of lava samples for Pb and Hf

isotope analysis were performed at the University of Iceland metal-free clean laboratory using the methods of Kamber and Gladu (2009) and Münker et al. (2001), respectively. For analyses performed at University of Iceland, analytical procedures were identical to those in Halldórsson et al. (2022), which used Tl-doping to correct for mass-fractionation during MC-ICP-MS analyses. Leaching, digestion, separation, and analysis of reference materials AGV-2 ($n = 4$) and BCR-2 ($n = 4$) in Iceland obtained average Pb isotope ratios within uncertainty of those of Todd et al. (2015), see Table S5 in Supporting Information S2. In Münster, chemical separation and isotope analysis procedures of Hf and Pb isotope measurements followed those of Sani et al. (2024) and Todd et al. (2015), respectively. All Hf isotope data are normalized to JMC475 and reported relative to $^{176}Hf/^{177}Hf = 0.282160$ (Blichert-Toft et al., 1997). All Pb isotope measurements were reduced using the NBS981 composition of Baker et al. (2004). Unleached aliquots of BCR-2 were measured at Münster for Hf ($n = 4$) and Pb ($n = 1$) isotope compositions and are within uncertainty of those determined by Weis et al. (2007) and Todd et al. (2015), respectively. Sample G20210321-2 was measured for Pb isotope ratios in both the Münster and Iceland laboratories, and the results agree within analytical uncertainty, see Table S5 in Supporting Information S2. Uncertainties given in plots represent either the standard error of analysis or the standard error of the average of multiple duplicates, whichever is greater.

4.2. Thermobarometry Methods

Pressures of magma storage were estimated using both clinopyroxene-melt (cpx-melt) and Olivine-Plagioclase-Augite-Melt (OPAM) barometric methods. The clinopyroxene–melt barometer of Neave and Putirka (2017) (SEE = ±1.4 kbar, i.e. ±4.9 km) implemented in Thermobar (Wieser et al., 2022) was used. In the cpx-melt barometry calculation, 628 clinopyroxene measurements from the 2021 Fagradalsfjall lavas were tested for equilibrium with liquid compositions derived from macrocryst-free matrix ($n = 14$), matrix glasses ($n = 374$), and melt inclusions compositions (MI; $n = 199$). The macrocryst-free matrix and matrix glass compositions are presented in this study, and the MI compositions are from Halldórsson et al. (2022). Equilibrium criteria include: (a) Observed DiHd, EnFs and CaTs component values within ±0.06, ±0.05 and ±0.03 of predicted values, respectively (Neave, Bali, et al., 2019), (b) Kd $\frac{Fe-Mg}{Cpx-Liq}$ values within ±0.03 of equilibrium values calculated using Eq. 35 from Putirka (2008), (c) Melt $Fe^{3+}/Fe_T = 0.15$, and (d) exclusion of clinopyroxene compositions with Al (6O) < 0.11, to account for sector zoning (Neave & Putirka, 2017). In total, 451 clinopyroxene compositions were successfully matched with equilibrium liquids. OPAM barometry (SEE = 1.1 kbar, i.e. ±3.9 km) used the new calibration of Higgins and Stock (2024).

In the OPAM pressure calculations, 374 matrix glass compositions (including both tephra and quenched lava) and 36 macrocryst-free matrix compositions from 16 different samples were used. As a test, OPAM saturation was tested by using two different statistical approaches to screen out melt compositions that do not lie on the OPAM boundary: the probability of fit test by Baxter et al. (2023) and the $OPAM_{SAT}$ test by Higgins and Stock (2024). The two approaches filtered out different samples, but both sets of filtered samples record the same observations, and therefore the filtering methods do not affect the conclusions (See Figure S5 in Supporting Information S1).

5. Results

5.1. Petrography

Lava samples from the 2021 Fagradalsfjall eruption are variably vesicular and phyric in hand specimen (Figure 2). The vesicularity of a given sample varied depending on the type of flow, the height within the flow, and the proximity to the vent. For example, the tops of vent-proximal pahoehoe flows were strongly vesicular and foam-like, whereas the cores of *a′a* flows or distal pahoehoe flows might be nearly devoid of vesicles. The 2021 lavas contain macrocrysts (>1 mm), microcrysts (0.1–1 mm) and microlites (<0.1 mm) of plagioclase, olivine, clinopyroxene and Cr-spinels. The macrocryst modal abundances of the samples have not been determined quantitatively, but are approximately 10 vol%. The lavas typically contain macrocrysts of plagioclase and olivine along with rarer macrocrysts of clinopyroxene (Figure 2a).

Plagioclase macrocrysts are up to 2 cm in diameter (typically ∼5 mm) and are typically euhedral (Figure 2b). Olivine is up to 5 mm in diameter (typically ∼2 mm), and is likewise typically euhedral (Figure 2c). Clinopyroxene ranges up to 5 mm and is mostly round and anhedral with significant evidence of resorption (Figure 2d). Clinopyroxene crystals decreased in abundance throughout the eruption. Cr-spinel ranges up to 0.2 cm in

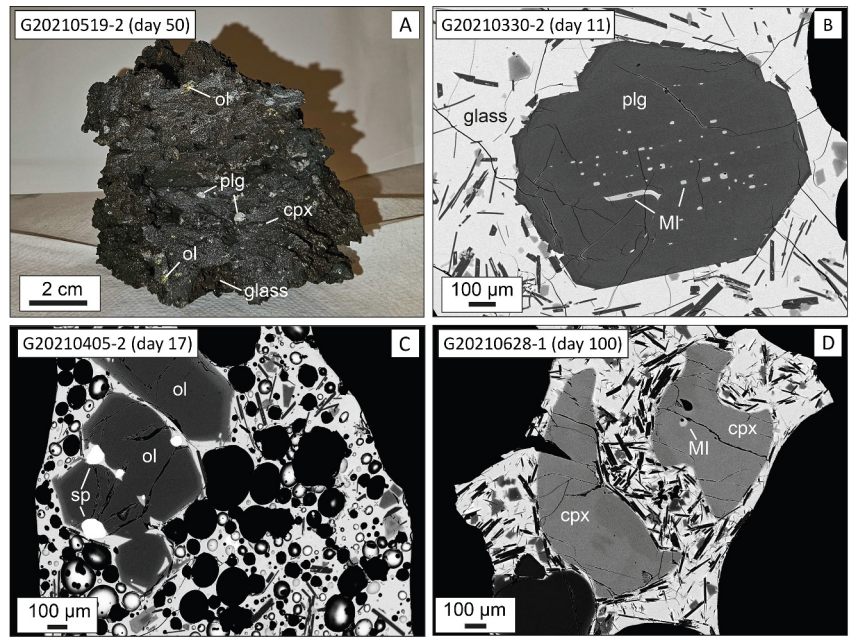

Figure 2. Petrographic features of the 2021 Fagradalsfjall eruption products. The upper left of panels (a–d) is the sample ID for the sample and the sample eruption day. (a) A photograph of a representative hand specimen of unquenched 2021 lava. Macrocrysts can be seen at this scale. (b) A back-scattered electron (BSE) image of a plagioclase (plg) macrocryst and melt inclusions (MI). Note thin low-An (dark-colored) rim. (c) A BSE image of olivine (ol) and spinel (sp) crystals in a tephra sample. Note the low-Fo (light-colored) rim. (d) A BSE image of clinopyroxene (cpx) crystals and a melt inclusion (MI). Note resorbed shape and lack of rim.

diameter and it is found both as a microcryst phase and as inclusions in olivine crystals (Figure 2c). All macrocryst phases contain glassy melt inclusions, mainly located in the cores of the macrocrysts. The lava also contains rare gabbroic and anorthositic xenoliths.

5.1.1. Plagioclase, Olivine, and Clinopyroxene Mineral Chemistry

Plagioclase macrocrysts are characterized by patchy or complexly zoned high-An cores surrounded by thin low-An rims. The contact between core and rim zones is sharp. The anorthite content of plagioclase cores varies between $An_{76–91}$, with most compositions being in the range $An_{84–89}$. Plagioclase rims are in the range An_{78-87}, with most of them being between $An_{78–84}$, overlapping with the composition of microlites and microcrysts (Figure 3a). The distribution of plagioclase compositions does not appear to shift over the course of the eruption (Figure 3a).

Olivine macrocrysts are typically normally zoned with high-Fo cores surrounded by lower Fo rims (Figure 3b). A gradational contact is observed between core and rim. Reversely zoned olivine macrocrysts do occur but are rare. In the eruption products, olivine core compositions range between $Fo_{84–90}$, with the majority having $Fo_{87–89}$. Olivine compositions are relatively consistent through the eruption, although they may decline slightly at the end. Relatively evolved olivine cores, with Fo_{84-86}, occur sporadically throughout the eruption. Most olivine rim compositions from the 2021 products range between $Fo_{84–87}$ (for more details on olivine macrocrysts, see Kahl et al., 2023).

Clinopyroxene macrocrysts are either unzoned or sector zoned, commonly displaying a sharp contact between sectors. The composition of clinopyroxene macrocrysts ranges between $Mg\#_{82–91}$, with the majority of compositions being in the range $Mg\#_{84–88}$ and Cr_2O_3 between 0.5 and 1.5 wt%. There is no significant variability in clinopyroxene Mg# throughout the eruption, except for clinopyroxene erupted around day 100 which, on average, are in the range $Mg\#_{86–91}$ (Figure 3c).

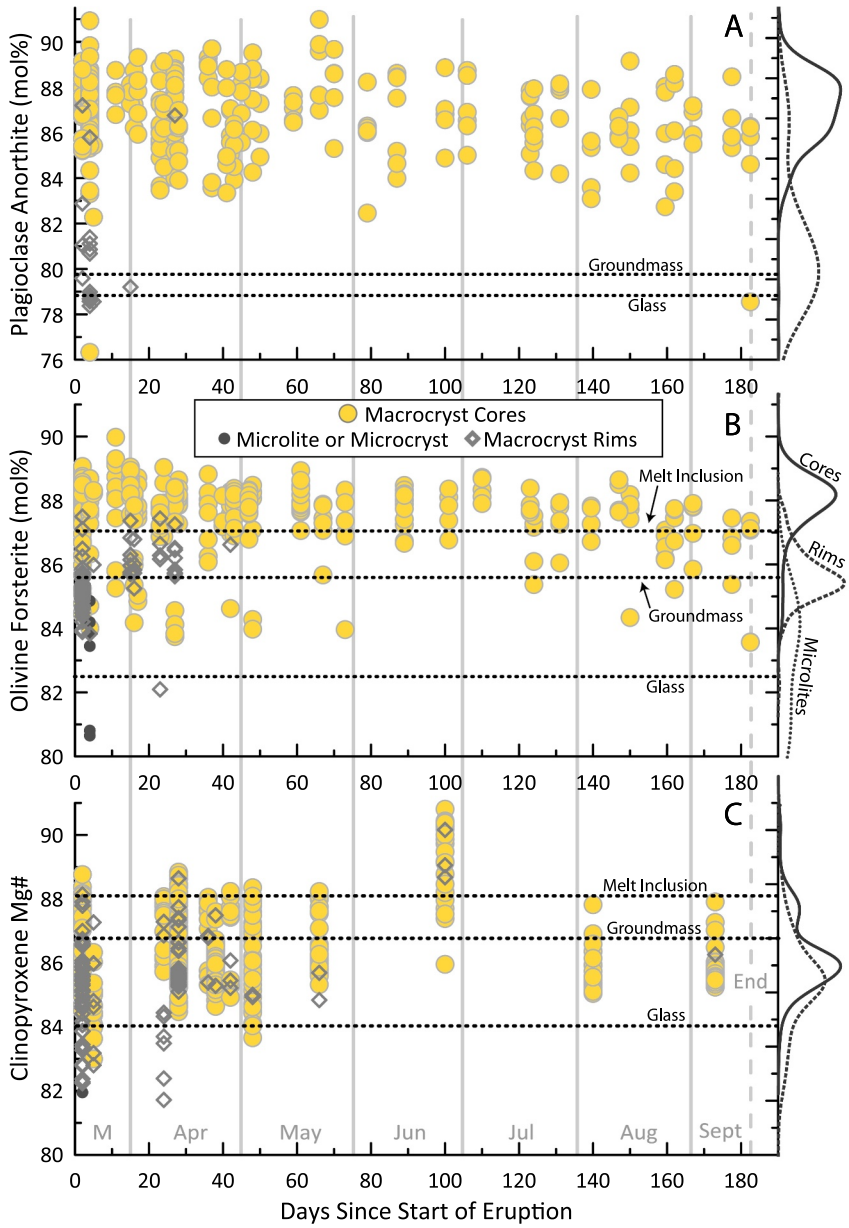

Figure 3. (a) Plagioclase anorthite content, (b) olivine forsterite content, (c) and clinopyroxene Mg# versus eruption date. The measured compositions of macrocryst cores (large yellow circles), macrocryst rims (lighter gray diamonds), and microlites and microcrysts (small darker gray circles) are plotted. On the right of each figure are three kernel density estimations (KDEs) of macrocryst cores (solid black line), macrocryst rims (dashed line), and microlites and microcrysts (fine dotted line). The horizontal dashed black lines represent the An, Fo, and Mg# of cpx compositions that are in equilibrium with compositions of the average lava glass, macrocryst-free matrix (groundmass), and melt inclusions. The plagioclase equilibrium line for melt inclusions is not shown because of the complexities of high-An plagioclase-melt phase equilibria (see Ustunisik et al., 2021). Plagioclase equilibrium was calculated using the model of Neave and Namur (2022). Olivine equilibrium was achieved by using a Fe-Mg Kd in the range 0.27–0.33 (Roeder & Emslie, 1970), whereas for clinopyroxene in the range 0.24–0.30 (Putirka, 2008).

5.2. Lava Geochemistry

5.2.1. Major Elements in Whole Rock, Macrocryst-Free Matrix, and Glass

The glasses have MgO concentrations that range from 6.8 wt% (quenched a'a glass) to 8.7 wt% (fountaining tephra) (Figure 4). Glasses have lower MgO than the whole rock and macrocryst-free matrix from the same

10.1029/2024AV001310

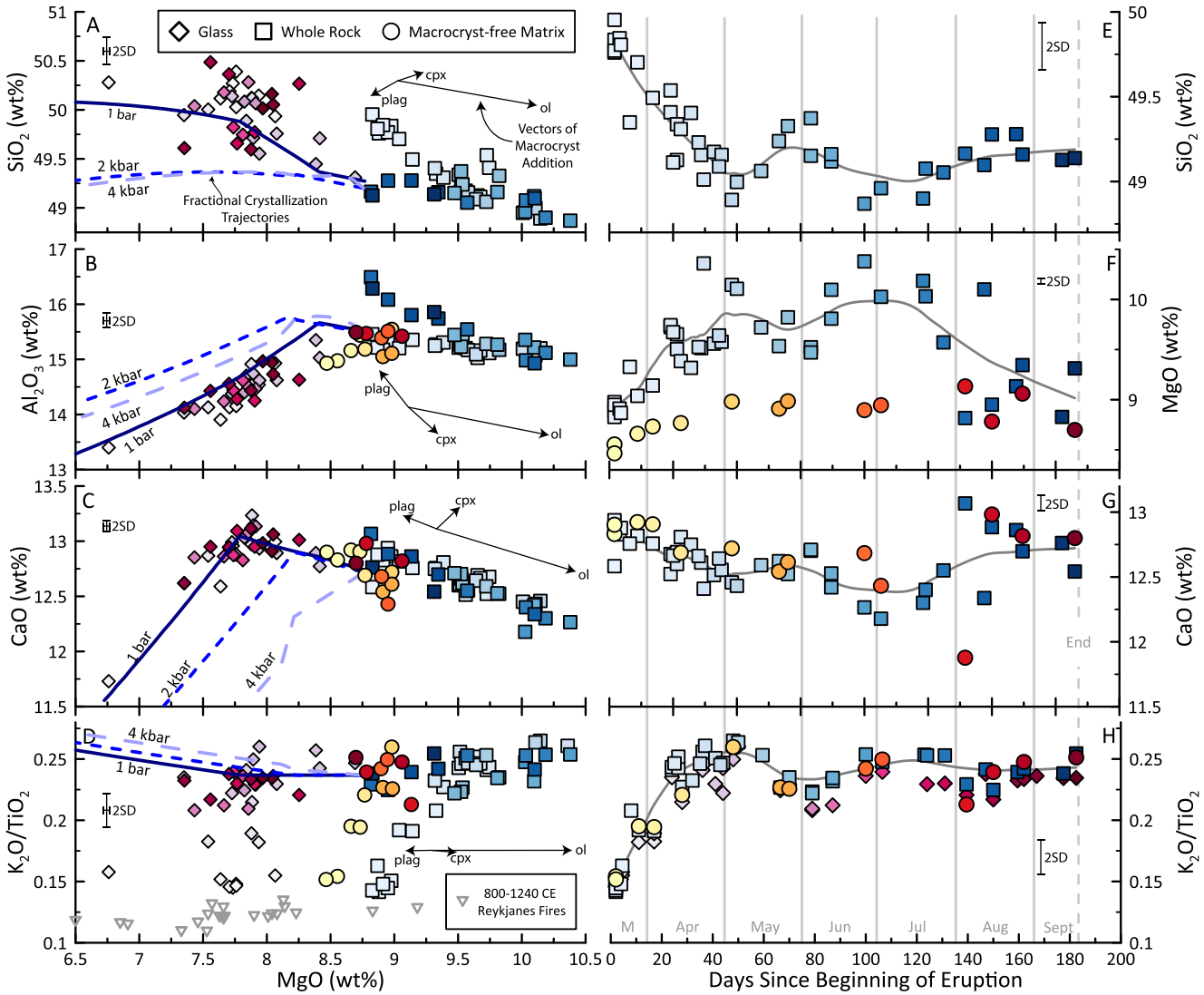

Figure 4. (left) MgO versus SiO_2 (a), Al_2O_3 (b), CaO (c), and K_2O/TiO_2 (d). (right) Eruption day versus SiO_2 (e), MgO (f), CaO (g), K_2O/TiO_2 (h). Symbol shapes define different analysis types: squares are whole rock, circles are macrocryst-free matrix, and diamonds are average glass composition. Symbol colors change with time where darker is later in the eruption, see symbol colors in panels (e, f, g, h). Analytical uncertainty is given by the error bar in each plot. The arrows in (a–d) indicate vectors of macrocryst addition, with the length of the vector corresponding to 2.5% addition of an average macrocryst. Blue solid and dashed curves represent Petrolog3 (Danyushevsky & Plechov, 2011) fractional crystallization models at 1 bar, 2 kbar, and 4 kbar, using the average macrocryst-free matrix as a starting composition with 0.2 wt% H_2O. Mineral/melt models for olivine, plagioclase and clinopyroxene are from Danyushevsky (2001). In panels (e, f, g, and h), the gray line is a local regression fit of the whole rock compositions through time. Macrocryst-free matrix is not plotted in (a and e) because of SiO_2 contamination from hand grinding. As glass compositions are controlled by surface crystallization, they do not display coherent temporal variation for SiO_2, Al_2O_3, or CaO and are not included in (e, f, or g). The data for the 800–1240 CE Fires in (d) is from Peate et al. (2009).

samples. Glass SiO_2, Al_2O_3, and CaO falls along a 1 bar fractional crystallization curve (Figure 4) that uses the average macrocryst-free matrix as a starting composition.

The whole rocks have MgO concentrations that range from 8.8 wt% to 10.4 wt% (Figure 4), higher MgO content than either glasses or macrocryst-free matrix. The compositions display coherent changes over time (Figures 4e–4h). For example, SiO_2 content decreases from ~49.8 to 49.0 wt% in the first 50 days of the eruption, and then has lower amplitude oscillatory change from day 50 until the end of the eruption, matching trends observed in K_2O/TiO_2 space (see Figure 4h). Although whole rock MgO also increases in the first days of the eruption, it decreases substantially toward the end of the eruption at day ~140 (Figure 4f). This decrease in whole rock MgO is matched by a sudden increase in whole rock CaO. Whole rock compositions show a strong correlation between CaO and

MgO that falls along the olivine and plagioclase macrocryst addition/subtraction vector but is nearly perpendicular to the clinopyroxene macrocryst addition vector (Figure 4c).

Macrocryst-free matrix analyses have MgO concentrations that range from 8.5 to 9.1 wt%, which is intermediate between the glass and whole rock MgO contents (Figure 4). Macrocryst-free matrix shows less major element compositional variability than either glass or whole rocks, but distinct change in composition over time is clear in MgO and CaO. MgO displays the greatest change in the first 50 days of the eruption, and then remains about constant for the rest of the eruption. The first lavas have macrocryst-free matrix compositions with lower MgO than lavas erupted after day 50.

In general, the major element compositions of the Fagradalsfjall lavas are dissimilar to the lavas erupted in the 800–1240 CE Fires, and all Reykjanes Peninsula lavas more generally. The lavas have higher whole rock MgO contents (8.8–10.4 wt%) than lavas from the 800–1240 CE Fires (6.5–9.2 wt%; Peate et al., 2009). They also have higher K_2O/TiO_2 (0.14–0.26) than the 800–1240 CE Fires lavas (0.11–0.13; Peate et al., 2009), and nearly all other Reykjanes Peninsula basalts (Figure 4d, Figure S6 in Supporting Information S1).

5.2.2. Trace Element Composition of the Macrocryst-Free Matrix

The variability in the concentration of a given trace element in the macrocryst-free matrix increases with its degree of incompatibility (Figure S1 in Supporting Information S1). Highly incompatible elements like U are highly variable (U ranges from 0.11 to 0.25 ppm, a relative difference of 127%), while somewhat less incompatible elements like Zr show less variability (Zr ranges from 49.9 to 71.1 ppm, a relative difference of 42%). Moderately incompatible elements such as Yb have even smaller variabilities (Yb ranges from 1.94 to 2.14 ppm, a relative difference of 10%). The compatible element Ni is an exception to this trend, displaying variability (excluding analyses affected by Ol addition/subtraction, Ni has a range of 43%) similar to Sr. We find that the observed variability in moderately incompatible elements (Li, Sc, Y, Tb, HREEs) is small enough that it is not discernible from analytical noise, and therefore the variability of these elements is not discussed further (see Supplementary Information for statistical procedure). The moderately incompatible elements aside, all elements form strong positive linear correlations with one another (Figure S2 in Supporting Information S1).

Incompatible trace element (ITE) ratios also show wide variabilities in the 2021 Fagradalsfjall eruption. Ratios such as La/Sm, La/Yb, or Nb/Zr range from 1.93 to 3.06, 2.13 to 4.45, and 0.12 to 0.18, respectively (relative differences from 50% to 110%). The variability in La/Sm or Nb/Zr is larger than that observed in all historic lavas from the Reykjanes Peninsula (see Figure S6b in Supporting Information S1). However, ratios of highly incompatible elements such as Ba/Th, Nb/La, or Th/Nb show less variability (relative difference around 13%).

Bivariate plots of ITE concentrations, ITE ratios, and Ni show very strong, positive correlations (Figure 5). Correlations between two highly ITE elements generally have a squared correlation coefficient, R^2, higher than 0.98 (Figure 5a). As shown in Figures 5a–5d, sample compositions fall close to apparent binary mixing trends. ITE concentrations also form a negative correlation with whole rock SiO_2 and a positive correlation with macrocryst-free matrix MgO (Figure S7 in Supporting Information S1).

Concentrations of ITEs and Ni, as well as incompatible minor elements like K_2O and TiO_2, and their ratios, fluctuate coherently over time in the eruptive products (Figure 6). As also observed by Halldórsson et al. (2022), both lava ITE concentrations and their ratios increase during the first 50 days of the eruption. Beyond this period, ITE concentrations exhibited smaller and shorter amplitude oscillatory variations until the eruption's end. The temporal variations between different ITEs and ratios are well-correlated, as is expected from the strong correlations present on bivariate plots.

The 2021 Fagradalsfjall lavas frequently display trace element compositions that are highly unusual for Icelandic lavas. For example, their Nb/Zr – Sm/Yb compositions plot outside the field of all measured erupted Icelandic basalts (Figure 7a). Similarly, the range of some ratios of highly incompatible elements (e.g., Th/La) do not overlap with that of Reykjanes Peninsula basalts (Figure S6c in Supporting Information S1). The early-erupted, ITE depleted Fagradalsfjall lavas have some trace element similarities to ITE depleted Reykjanes Peninsula basalts- for example, their Sm/Yb – La/Sm compositions are similar. In contrast, ratios of highly to moderately incompatible elements in Fagradalsfjall basalts (e.g., Nb/Zr, Rb/Sr, La/Sm, and K_2O/TiO_2) reach values higher than nearly any other Icelandic rift basalt, and have values more similar to off-rift basalts (e.g., Figures 4d and 7a, Figure S6b in Supporting Information S1).

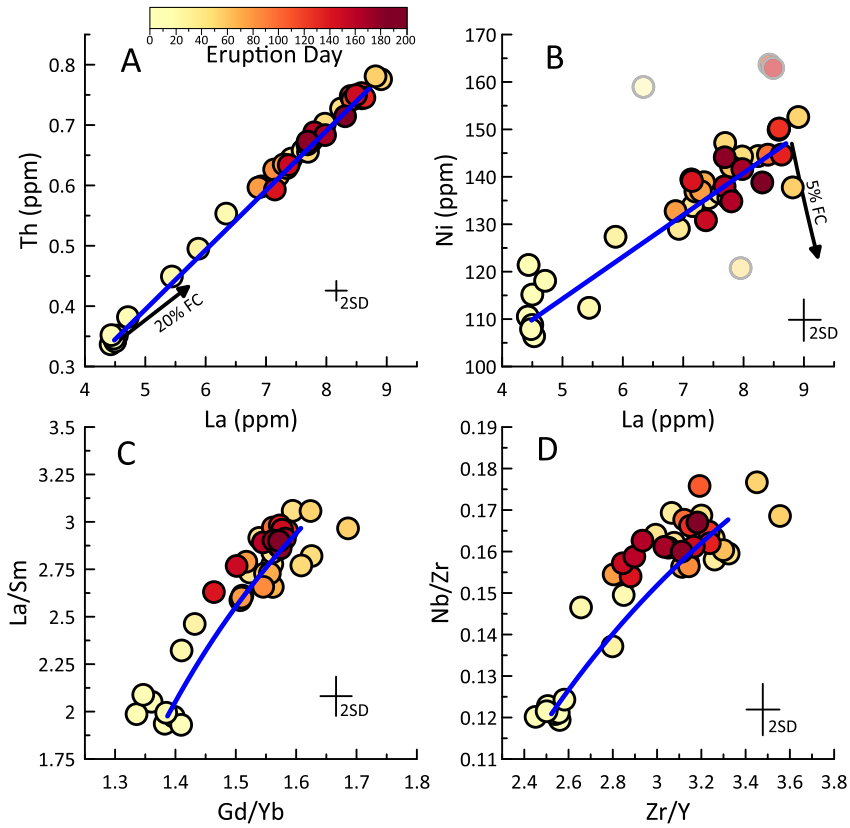

Figure 5. Bivariate plots of trace elements in macrocryst-free matrix. Symbol color changes with eruption day, see color bar. The blue line represents a binary mixing line that use the five most and least enriched samples (see Supporting Information S1). Four samples, grayed out in panel (b) have likely experienced olivine addition/subtraction. The crosses in panels (a–d) represent 2 SD analytical uncertainties. (a) The black arrow shows the effect of 20% fractional crystallization or (b) 5% fractional crystallization. The effect of 20% fractional crystallization in panels (c) and (d) is similar to the symbol size and not plotted. The plots show that the trace element variation present in the macrocryst-free matrix is dominantly explained by mixing.

5.2.3. Radiogenic Isotope Ratios

The 2021 Fagradalsfjall eruption lavas have variable Sr, Nd, Hf, and Pb isotope ratios (Figures 8 and 9). The ratios $^{87}Sr/^{86}Sr$, $^{143}Nd/^{144}Nd$, $^{176}Hf/^{177}Hf$, and $^{206}Pb/^{204}Pb$ range from 0.703107 to 0.703209, 0.512949 to 0.513017, 0.283172 to 0.283234, and 18.7184 to 18.8501, respectively (Figures 8–10). Relative to lavas erupted during the 800–1240 CE Fires, the 2021 Fagradalsfjall eruption exhibits a range in isotope composition that is 224%, 400%, and 20% greater in terms of $^{87}Sr/^{86}Sr$, $^{143}Nd/^{144}Nd$, and $^{206}Pb/^{204}Pb$, respectively (Peate et al., 2009). All investigated radiogenic systems form statistically significant linear correlations with ITE concentrations, but $^{87}Sr/^{86}Sr$ and $^{206}Pb/^{204}Pb$ correlate with ITE concentrations especially well (i.e., for La, $R^2 > 0.95$).

Radiogenic isotope ratios change coherently over time (Figures 8 and 9, Figure S8 in Supporting Information S1). All investigated radiogenic isotope systems change significantly during the first 40 days of the eruption but thereafter show smaller oscillatory changes, like the behavior of ITEs (Figure 8). The temporal variability divides the sample set into three different groups. Samples erupted during days 0–7 have higher $^{143}Nd/^{144}Nd$ and $^{176}Hf/^{177}Hf$ than the other samples (Figures 9a, 9c, and 9d), and also fall off the trend made by the other samples in $^{207}Pb/^{204}Pb - ^{208}Pb/^{204}Pb$ space (Figure 9b). Samples erupted during days 8–44 span a wider range of isotope compositions than the other groups and form a nearly perfect linear trend on any plot of radiogenic isotope compositions (Figures 9a–9d). Samples erupted during days 45–183 have higher $^{87}Sr/^{86}Sr$ and $^{206}Pb/^{204}Pb$ but lower $^{143}Nd/^{144}Nd$ and $^{176}Hf/^{177}Hf$ than the lavas from days 0–7, and in $^{87}Sr/^{86}Sr - ^{143}Nd/^{144}Nd$ space, form a linear trend that is separate and parallel from the one made by the samples from days 8–44 (Figure 9a).

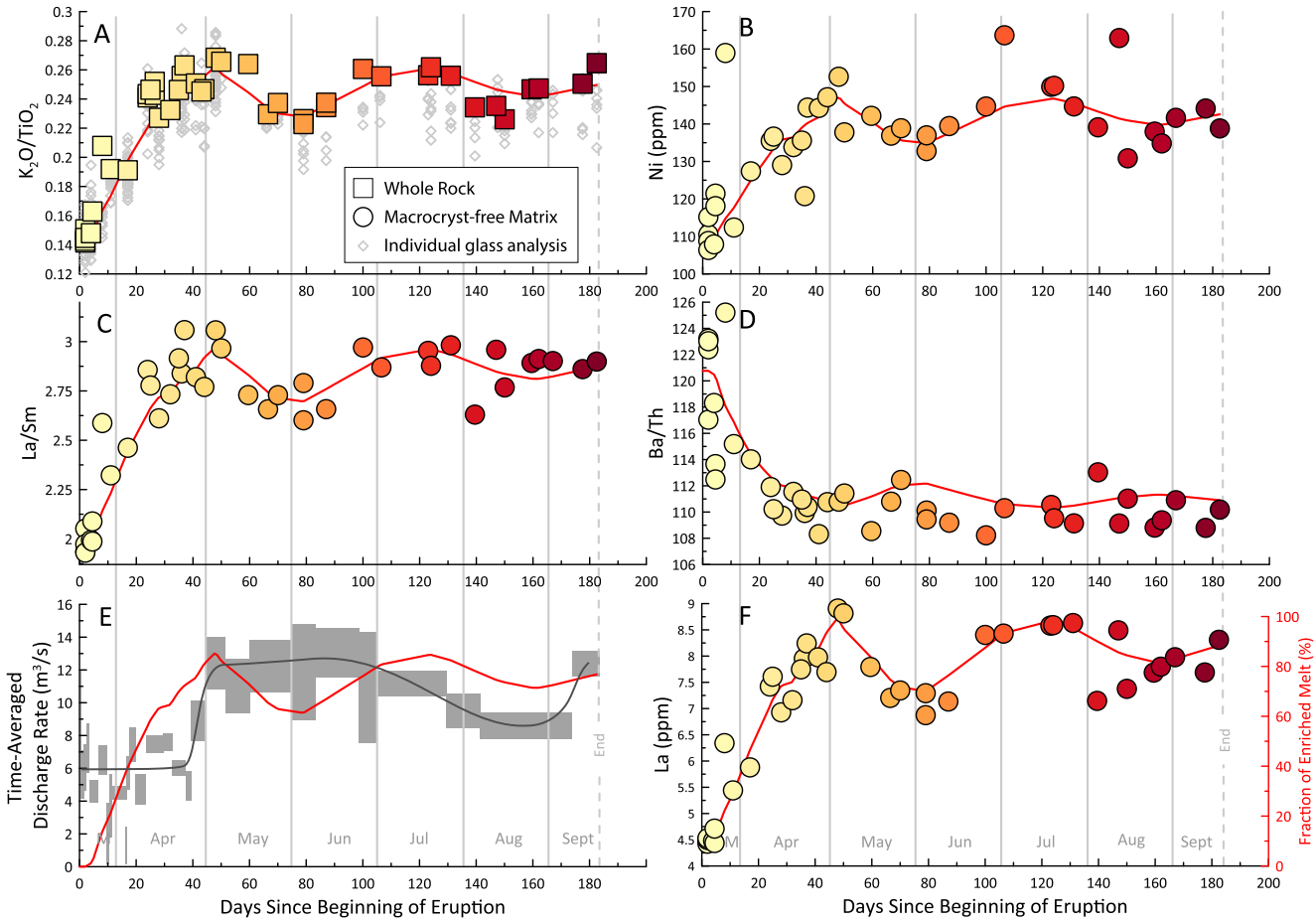

Figure 6. (a, c, and d) Eruption day versus different incompatible trace element ratios, (b and f) trace element concentrations, and (e) time-averaged discharge rate of lava during the eruption (Pedersen et al., 2022). Square symbols indicate whole rock analyses, circles indicate macrocryst-free matrix, and diamonds indicate individual glass analyses. Symbol colors correspond to the eruption day and darken with time, as in Figure 5. All plots include a red curve which represents a binary mixing model calculated from a local regression fit of the La concentration (panel (f); see Supporting Information S1). The red curve therefore represents the composition for that chemical parameter as predicted by La. The good correspondence between the red curve and the different systems in panels (a–d) shows that different trace element systems are highly correlated in the 2021 lava and their behavior can therefore be predicted from La concentration. In panel (e), the gray boxes represent the estimated range of effusion rate at a given time period and the curved gray line represents a fit of the effusion rate estimates over time. The red line in panel (e) is the fit of the La data from panel (f), and is included for reference.

The Sr, Nd, Hf, and Pb isotope ratios of the 2021 Fagradalsfjall lavas reveal a distinct compositional signature unlike any previously observed Icelandic lava. For example, $^{143}Nd/^{144}Nd$ in the 2021 lavas with the highest ITE concentrations are the lowest published for any Icelandic rift lava (Figure 10a; Harðardóttir et al., 2022). Similarly, all 2021 lavas have the highest $^{176}Hf/^{177}Hf$ at a given $^{143}Nd/^{144}Nd$ of any measured Icelandic basalt except for highly depleted Reykjanes Peninsula picrites (Figure 10b). For comparison, two Reykjanes Peninsula lavas that also have extremely low $^{143}Nd/^{144}Nd$ are bolded in Figures 10a, 10c, and 10d. In contrast, the Sr and Pb isotope ratios of the 2021 Fagradalsfjall lava are similar to those erupted in the 800–1240 CE Fires (Figures 10c and 10d, Figures S6d and S6e in Supporting Information S1; Peate et al., 2009; Thirlwall et al., 2004).

5.2.4. Thermobarometry Results

Calculated cpx-melt pressures for clinopyroxene macrocrysts in the 2021 Fagradalsfjall eruption range from 0 to 5 kbar (0–18 km; pressures are converted into depths assuming an average crustal density of 2.86 g/cm^3, Carlson & Herrick, 1990). Most fall within a 2.5–3.5 kbar (9–13 km) range and there is no significant temporal change in pressure since the eruption's onset in 2021 (Figure 11a). Overall, the average crystallization pressure of clinopyroxene crystals across all samples is 3.0 ± 0.6 kbar (10.4 ± 2.1 km). Note that the uncertainty of the cpx-melt

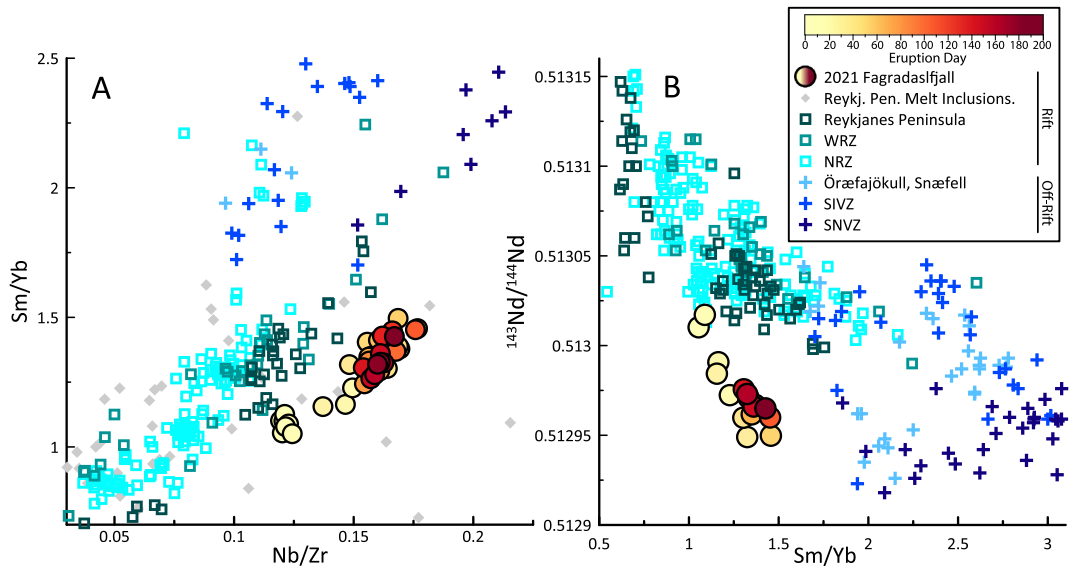

Figure 7. Nb/Zr versus Sm/Yb (a) and Sm/Yb versus $^{143}Nd/^{144}Nd$ (b) for compiled Icelandic basalts, melt inclusions, and the 2021 Fagradalsfjall lavas. The 2021 Fagradalsfjall symbol colors correspond to eruption date, see color bar. Literature data are basaltic samples with high quality isotope analyses from the compilation of Harðardóttir et al. (2022). Reykjanes Peninsula melt inclusions are from the studies of Halldórsson et al. (2022) and Maclennan (2008a). WRZ, NRZ, SIVZ, and SNVZ are rift and off-rift zones in Iceland: Western Rift Zone, Northern Rift Zone, South Iceland Volcanic Zone, and Snaefellsnes Volcanic Zone, respectively (see Harðardóttir et al., 2022). These plots show how the 2021 Fagradalsfjall lavas are compositionally unlike almost all Icelandic basalts, as they plot outside the compositional extent of erupted Icelandic basalts.

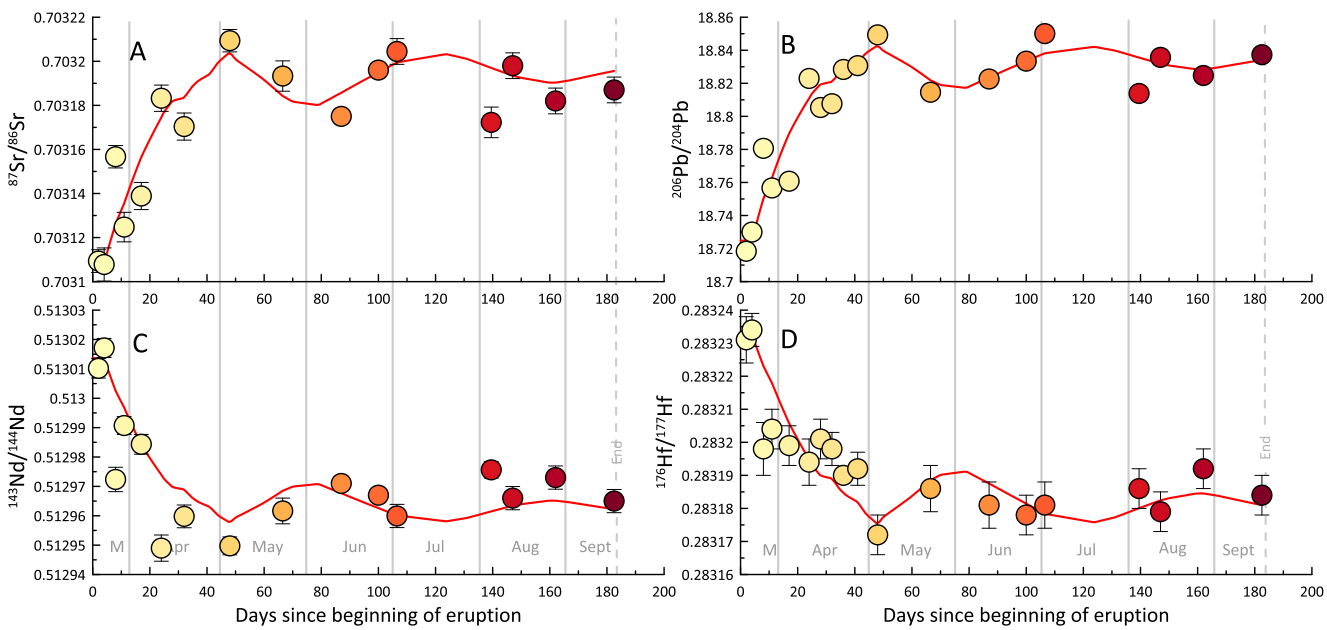

Figure 8. Eruption day versus radiogenic isotope compositions: eruption day versus (a) $^{87}Sr/^{86}Sr$, (b) $^{206}Pb/^{204}Pb$, (c) $^{143}Nd/^{144}Nd$, and (d) $^{176}Hf/^{177}Hf$. Symbol color darkens with time, as in Figure 6. The red line represents the [La]-based mixing model introduced in Figure 6, and represents the predicted isotope composition based on [La] (see Figure 6 caption, Supporting Information S1). Although radiogenic isotope compositions generally follow the red mixing trend, like trace elements, they sometimes display compositions that do not fit binary mixing within uncertainty (e.g., panel (c)).

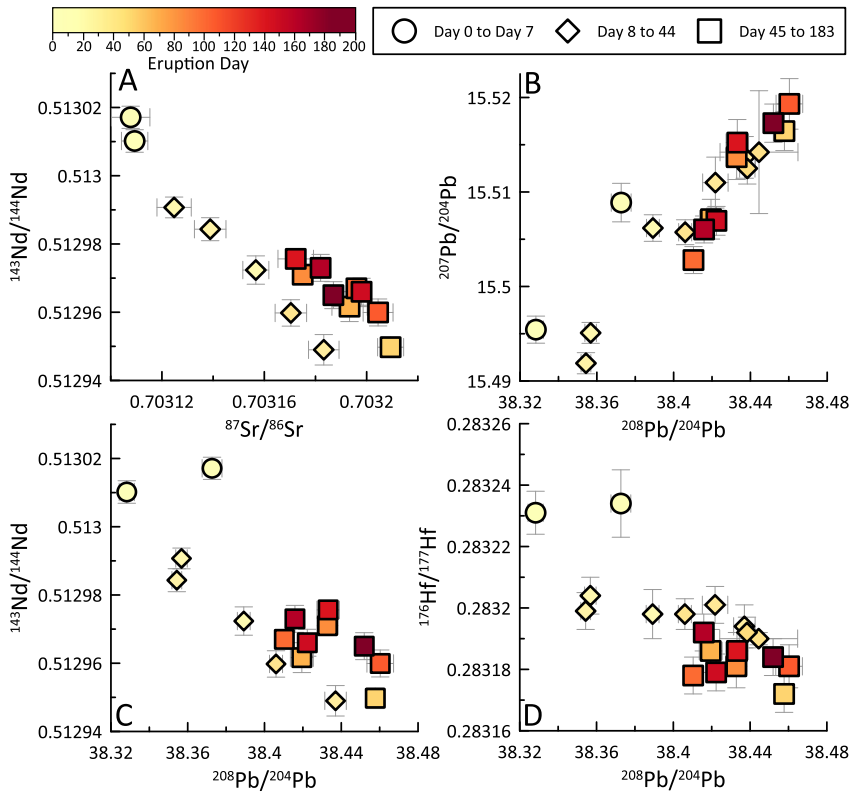

Figure 9. (a) $^{87}Sr/^{86}Sr$ versus $^{143}Nd/^{144}Nd$, (b) $^{208}Pb/^{204}Pb$ versus $^{207}Pb/^{204}Pb$, (c) $^{208}Pb/^{204}Pb$ versus $^{143}Nd/^{144}Nd$, and (d) $^{208}Pb/^{204}Pb$ versus $^{176}Hf/^{177}Hf$. Symbol color darkens with time as given in the color bar, and symbol type is divided into three temporal groups as given in the legend. This plot illustrates the changes in radiogenic isotope composition that occur over the course of the eruption. Note that samples from days 0–7 have quite different compositions from one another and from the other samples, highlighting the rapid geochemical changes occurring in the first days of the eruption. Samples from day 8–44 form a nearly linear array in all isotope plots (a)–(d). Samples from day 45–183 are offset from the day 8–44 samples in (a), showing the sudden change in radiogenic isotope composition occurring at day ~45.

barometer is ±1.4 kbar (i.e., ±4.9 km, 1 SD) and therefore that the uncertainty of the barometer is larger than the range of the data (Neave & Putirka, 2017).

OPAM estimates for glass throughout the eruption suggest mean equilibration pressures of 0–2.7 kbar, with most of the pressures being 1–2 kbar (Figure 11b). Considering the uncertainty on the barometer (±1.1 kbar, i.e. ±3.9 km, 1 SD; Higgins & Stock, 2024), this is consistent with the observation that glass compositions from the eruption lie along 1 bar FC trend (Figure 4). The sole exceptions to this are tephra glasses erupted during the fountaining phase on days 37, 44 and 48, which record mean pressures between 3.5 and 4.5 kbar.

OPAM applied to macrocryst-free matrix compositions returns pressures in the range 3.1–5.6 kbar (10–20 km), which corresponds to a region spanning the lower crust to the mantle (Figure 11b). This range of pressures varies through the eruption, although within the uncertainty of the barometer. Macrocryst-free matrix samples erupted in the first weeks of the eruption record lower pressures, between 3.1 and 4 kbar (10–14 km; lower crust), whereas macrocryst-free matrix-based pressures from day 40 onwards record higher pressures in the range 4–5.6 kbar (14–20 km, spanning the lowermost crust and mantle). Macrocryst-free matrix pressures are higher than the cpx-melt pressures, except for the first weeks of the eruption, but broadly overlap in terms of barometer uncertainty throughout the eruption.

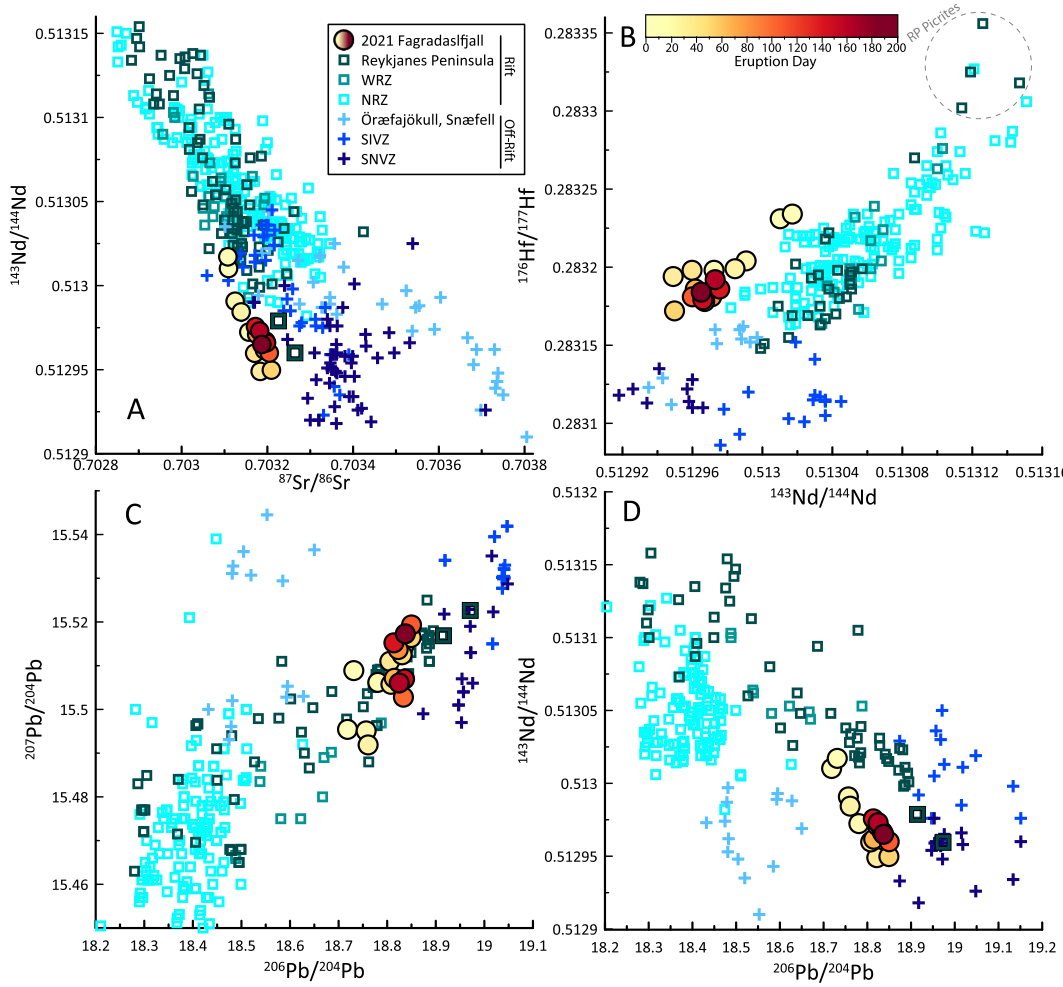

Figure 10. (a) $^{87}Sr/^{86}Sr$ versus $^{143}Nd/^{144}Nd$, (b) $^{143}Nd/^{144}Nd$ versus $^{176}Hf/^{177}Hf$, (c) $^{206}Pb/^{204}Pb$ versus $^{207}Pb/^{204}Pb$, and (d) $^{206}Pb/^{204}Pb$ versus $^{143}Nd/^{144}Nd$. Symbol color of 2021 Fagradalsfjall samples changes with eruption date, see color bar. Literature data are basaltic samples with high quality isotope analyses from the compilation of Harðardóttir et al. (2022). Bolded Reykjanes Peninsula samples to the right of the enriched Fagradalsfjall samples in (a), (c), and (d) are the highly enriched Reykjanes Peninsula samples discussed in the text with compositional similarities to the 2021 Fagradalsfjall lava. The Reykjanes Peninsula samples in gray circle in (b) are picritic lavas from Nicklas et al. (2021), as discussed in the text.

6. Discussion

6.1. Evidence for Syn-Eruptive Erosion of Crystal Mushes in the Lower Crust

Plagioclase and olivine macrocryst cores in 2021 Fagradalsfjall lavas are not in major-element equilibrium with their carrier melts, raising the possibility that they have been added to the magma during transport. Halldórsson et al. (2022) report that plagioclase, olivine, and clinopyroxene macrocryst-hosted melt inclusions in the 2021 lavas show compositions different from that of their carrier melt, and display wide incompatible element ratio variability. Additionally, Figure 3 shows that the average macrocryst-free matrix (which represents the melt composition prior to surface crystallization should be in equilibrium with olivine and plagioclase compositions of $Fo_{85.6}$ and $An_{79.8}$, respectively). However, the cores of the olivine and plagioclase macrocrysts are more primitive than the carrier melt, approximately Fo_{88} and An_{87}, respectively (see also Figures S9–S11 in Supporting Information S1). Although a primitive core and more evolved rim would be an expected consequence of fractional crystallization, the compositionally diverse melt inclusions in the macrocryst cores show that there is no such simple relationship between macrocrysts and their carrier melts. In contrast, the microlites and microcrysts likely crystallized out of the carrier liquid, as they are close to equilibrium with it (Figure 3, Figures S9–S11 in

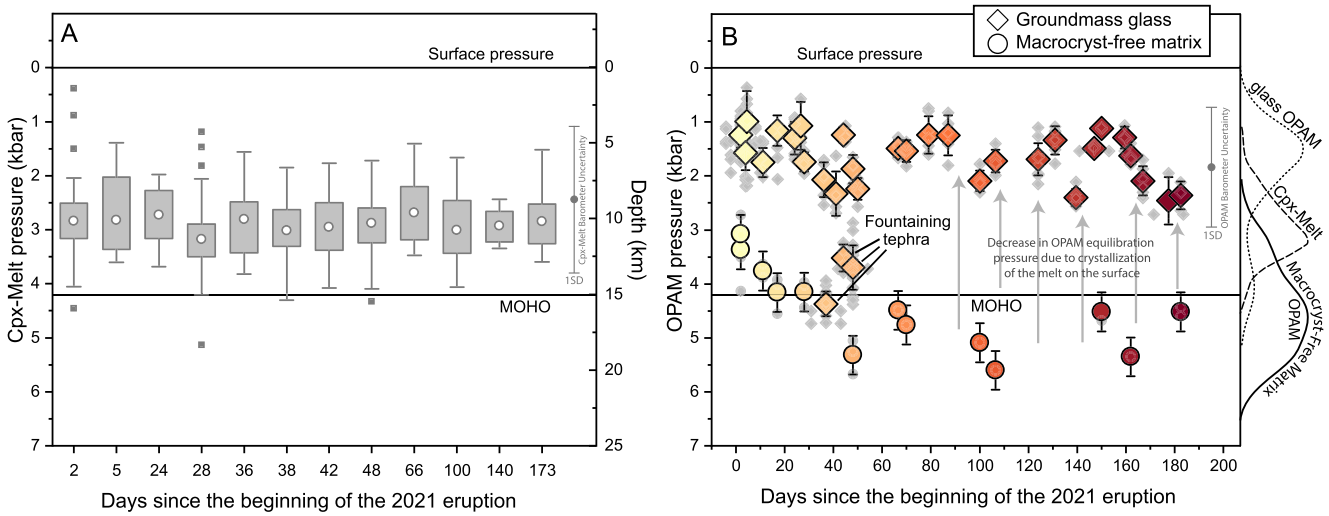

Figure 11. Plots of pressure estimates throughout the eruption. (a) Variation of clinopyroxene – melt pressures throughout the 2021 eruption. For each eruption day, the gray square boxes represent the interquartile-range, the white circles inside square boxes represent the mean, the ends of the whisker represent the limit of the 10% and 90% percentile. The small gray squares represent samples lying outside the whiskers. The 1 SD cpx-melt barometer uncertainty is given by the error bars on the on the right side of the plot. The pressures are converted into depths assuming an average crustal density of 2.86 g/cm^3 (Carlson & Herrick, 1990), and the depth to the crust-mantle boundary is based on the seismic estimates Weir et al. (2001). (b) Olivine-Plagioclase-Augite-Melt (OPAM) pressures calculated for in situ groundmass glass analyses (diamonds) and macrocryst-free matrix (circles). If multiple analyses are available for a given sample, the large symbol represents the average calculated OPAM pressure for each sample. The error bars represent 1σ analytical uncertainty (black whisker). The 1 SD barometer uncertainty is given by the error bars on the right side of the plot. OPAM estimates calculated from individual glass and macrocryst-free matrix analyses are displayed with small gray diamonds and circles, respectively. Symbols colors darken with eruption day. The curves on the right side of the plot represent KDE curves of glass (dotted line) and macrocryst-free matrix (solid line) OPAM estimates, and of clinopyroxene-melt pressures (dashed line). The gray arrows in (b) indicate the decrease in calculated OPAM pressure as lavas cool and crystallize on the surface.

Supporting Information S1). Together, this shows that the cores of the olivine, plagioclase, and clinopyroxene macrocrysts are not in equilibrium with their host melts and could not have directly crystallized from them.

If they didn't crystallize from their carrier liquids, the 2021 Fagradalsfjall macrocrysts must therefore represent materials added to the melt from another source. Given that settling velocities for mm-scale olivines in primitive basalts is rapid (~8.5 m/day; given a melt viscosity of 10 PaS, and 2 mm olivine diameter; Stokes, 1856), the macrocrysts were most likely entrained during transport, and therefore the presence of macrocrysts in the 2021 Fagradalsfjall lava represents a syn-eruptive erosion process at depth. Cpx-melt barometry shows lower pressures than OPAM macrocryst-free matrix pressures, potentially suggesting a somewhat lower pressure source depth for clinopyroxene crystals (and likely all macrocrysts) than the carrier melts. Two possible sources of macrocrysts include either crystal mushes or wallrocks disaggregating into the melt. Although xenoliths, which are more convincingly derived from subsolidus or very near solidus lower crust, do appear in the 2021 lavas, they are rare. A fraction of xenoliths are deformed, have recrystallized metamorphic textures, or have mineral core compositions more evolved than any macrocryst core, although most have compositions and igneous textures similar to the macrocrysts (Wenrich et al., 2022). However, there is no macrocryst population of deformed or evolved macrocrysts to compliment this population of xenoliths. Therefore, despite overlap in textures and compositions, the crustal sources of xenoliths and macrocrysts do not seem to be the exactly the same, which supports the idea that macrocrysts reflect entrained crystal mush. Most macrocrysts contain features showing derivation from high-porosity crystal mush bodies: (a) euhedral crystal shapes, (b) a lack of intracrystalline deformation, and (c) a diffusion timescale history that starts months or even years prior to eruption rather than during transport (see Kahl et al., 2023). The erosion of crystal mush from conduit walls causes widening of eruptive conduits and keeps eruptive conduits from closing, thereby prolonging eruptions (Sigmundsson et al., 2020). Therefore, the unusually long duration of the 2021 Fagradalsfjall eruption could therefore be in part due to this mush erosion process (Pedersen et al., 2022).

Recent work by Day et al. (2024) identified high bulk-rock $^{187}Os/^{188}Os$ and Pt/Ir ratios (the highest of any >50 ppb Os basalt in Iceland) in the earliest erupted lavas. Although Day et al. (2024) interpreted these geochemical features to be related to assimilation (i.e., melting of wall rock), we instead interpret them to be a feature of the

mush entrainment process, as assimilation of high fractions of refractory gabbroic wallrock is difficult to reconcile thermally with the primitive character of the Fagradalsfjall lava (Heinonen et al., 2022; see Supporting Information S1). Entrainment of macrocrysts at the crystal abundances we observe in the 2021 lavas (~10% macrocrysts) can explain why the earliest 2021 lavas have the highest $^{187}Os/^{188}Os$, as they have the lowest [Os] (Figure S4 in Supporting Information S1). Macrocryst entrainment also explains why the 2022 lavas do not have high $^{187}Os/^{188}Os$ ratios, as the 2022 lavas are crystal-poor and have experienced far less macrocryst entrainment (Caracciolo et al., 2024; Day et al., 2024). Furthermore, several of the investigated macrocrysts contain sulfides, and therefore can host non-negligible abundances of highly siderophile elements (Figure S3 in Supporting Information S1). We therefore attribute the high $^{187}Os/^{188}Os$ and Pt/Ir ratios of the 2021 lavas to reflect the accumulation of solid mush-derived macrocrysts within the lavas. Because the crystals are added to the melt in a solid state, they do not affect the composition of the glass or macrocryst-free matrix.

6.2. Constraints on the Depth of the 2021 Fagradalsfjall Magma Reservoir

Halldórsson et al. (2022) used thermobarometry on lavas, crystal cargoes, and volcanic gas emissions from the first 50 days of the 2021 Fagradalsfjall eruption to suggest a near-Moho reservoir as its source. In this section, we extend this analysis by applying thermobarometry to crystals and melts from the complete span of the 2021 Fagradalsfjall eruption, aiming for a more comprehensive understanding and more definitive location of its magma reservoir.

Pressures derived from in situ analysis of microlite-rich glass in the 2021 Fagradalsfjall eruption are unlikely to record pressures that represent magma reservoir storage pressures. Glasses crystallize as they cool on the surface following eruption and, following Caracciolo et al. (2023), this crystallization pushes OPAM pressures toward lower pressure estimates. This explains why glass compositions fall along a 1 bar fractional crystallization model curve (Figure 4). This also explains why only tephra erupted during high lava fountaining has glass compositions with higher OPAM pressures; because only tephra glasses were rapidly quenched in air before significant microlite crystallization could take place (Figure 11b).

As discussed in the previous section, the macrocryst crystal cargo likely represents crystal mush eroded from the conduit walls during magma transport. This places a constraint on the source of their ascending carrier melt because the carrier melt source cannot be shallower than the eroded material. This may explain why the cpx-melt and macrocryst melt inclusion H_2O-CO_2 saturation pressures (from Halldórsson et al., 2022) record pressures shallower than the Moho. However, the cpx-melt pressures are within uncertainty of the OPAM pressures, and the H_2O-CO_2 saturation pressures (the highest are ~3 kbar, ~12 km depth) represent minimum pressures of melt inclusion entrapment, and therefore these shallower calculated pressures do not exclude the crystal cargo from being derived close to Moho depths. Therefore, pressures from the macrocryst cargo could be consistent with the macrocryst-free matrix and tephra OPAM pressures (i.e., ~15 km), but a somewhat shallower source for the macrocrysts, even as shallow as 12 km, cannot be ruled out (Figure 11). The source of the magma, that is, the carrier melt, must be deeper than this 12 km limit.

Pressures derived from OPAM barometry of macrocryst-free matrix and rapidly quenched tephra glasses indicate that melts equilibrated at near-Moho pressures (~4 kbar or ~15 km depth) prior to eruption (Figure 11b). Although the beginning of the eruption records somewhat lower pressures than the rest of the eruption, these changes are well within the uncertainty of the barometer and their significance is not clear. If the change in calculated OPAM pressure corresponds to real changes in melt equilibration pressure, this difference could be the result of shallow equilibration of magmas in the pre-eruptive dike in the 3 weeks before the eruption began and/or that the early erupted lavas are derived from a separate magma body located at somewhat shallower depth (e.g., 12 km). Regardless, macrocryst-free matrix and tephra glass OPAM pressures are consistent with lower crustal to upper mantle pressures, and all are within uncertainty of Moho-like pressures.

Combined petrological and barometry-based constraints allow for evaluation of the location of the magma reservoir that sourced the 2021 Fagradalsfjall eruption. Though the OPAM barometer provides the best constraints we have on the pre-eruptive magma storage pressure, the range in pressure estimates (Figure 11b) is consistent with storage in a variety of locations: the lowermost lower crust, the Moho, or the mantle. The mantle itself is highly unlikely to be a significant source of magma directly to the eruption, as erupted macrocryst-free matrix compositions (representing the carrier melt prior to near-surface crystallization) are saturated in olivine, clinopyroxene, and plagioclase at near-Moho pressures. Near-primary magmas ascending from the mantle would

only be saturated in olivine and the erupted lava compositions require cooling and crystal fractionation in order to be saturated in all three mineral phases. Excluding the mantle, the lowermost crust and Moho remain as possibilities. Here, the composition of the crystal cargo of the 2021 lava can help constrain the pre-eruptive storage location of the magma. The Fagradalsfjall lava contains abundant olivine macrocrysts, which themselves have highly primitive compositions. As described in Section 6.1, these macrocrysts likely represent entrained material from crystal mushes. To identify the proportions of crystals in the eroded lithologies, tephra clasts from sample G20210428-1 were carefully crushed and all macrocrysts picked out and weighed. The clasts contained 83% olivine, 13% plagioclase, and 4% clinopyroxene macrocrysts by mass. This illustrates that the crystal cargo of Fagradalsfjall is nearly ultramafic, resembling an olivine-rich troctolite in terms of phase proportions. Note that crystal settling processes in magma would result in an overabundance of plagioclase, not olivine (see settling velocity calculation in Section 6.1). Therefore, the crystal mush supplying the Fagradalsfjall crystal cargo is equivalent to a highly mafic or ultramafic lithology: an olivine-rich troctolite or plagioclase-bearing dunite. Such primitive near-ultramafic lithologies are very rare in the shallow portions of ophiolites, but are common in the lowermost part of the lower crust or within the Moho transition zone (e.g., Oman ophiolite; Pallister & Hopson, 1981). As these crystals were likely entrained during transport, the magma reservoir may be deeper than the depth of crystal entrainment. We therefore infer that the magma bodies supplying the 2021 Fagradalsfjall eruption was located at the base of the lower crust or within the Moho transition zone.

6.3. Mantle Origins of the Geochemical Composition of the 2021 Fagradalsfjall Lavas

As originally remarked by Halldórsson et al. (2022), the 2021 Fagradalsfjall lavas contain an unusual degree of geochemical variability with respect to mantle tracers, greater than the geochemical variabilities of all other well studied individual MORB or OIB basalt flows globally. However, the trace element and radiogenic isotope compositions of the 2021 Fagradalsfjall lavas themselves are unusual, and reflect the distinctive nature of the Fagradalsfjall mantle source. In this section, we use the mantle geochemical terms "enriched" and "depleted," which require explanation for non-mantle geochemist readers. The terms "enriched" and "depleted" simply describe the high or low abundance of incompatible elements in a system, respectively. For example, a lava whose trace element and radiogenic isotope composition is "enriched" has high incompatible element contents compared to a group of reference lavas (in this study, typical Reykjanes Peninsula basalts), and has a radiogenic isotope composition consistent with long-term radiogenic ingrowth of an ITE enriched material in the mantle source (i.e., a high Rb/Sr mantle domain will gain high $^{87}Sr/^{86}Sr$ over time). These terms are useful because they describe the mantle-derived characteristics of lava, which reflect the mantle source and melting process. For example, enriched Icelandic basalts are formed at lower degrees of partial melting and at greater depth than depleted basalts (Harðardóttir et al., 2022).

Lavas erupted after day ~45 have highly enriched trace element and radiogenic isotope compositions. These lavas have the most enriched (i.e., the lowest) $^{143}Nd/^{144}Nd$ ever measured in an Icelandic rift basalt (Figure 10a). Additionally, the 2021 Fagradalsfjall lavas have very high $^{176}Hf/^{177}Hf$ at a given $^{143}Nd/^{144}Nd$, only similar to highly depleted Reykjanes Peninsula picrites (Figure 10b) and Nb/Zr – Sm/Yb compositions that do not plot within the field of compiled Icelandic basalts (Figures 7a and 7b). Combined, these features render all 2021 Fagradalsfjall lavas compositionally distinct from all well-characterized Reykjanes Peninsula basalts and Icelandic rift basalts in general.

Although the enriched compositions of the 2021 Fagradalsfjall lavas are certainly compositionally distinct, two lavas that previously represented the lowest $^{143}Nd/^{144}Nd$ of Icelandic rift basalts, have compositional similarities to the more enriched 2021 Fagradalsfjall lavas (Thirlwall et al., 2004). These two lava samples are only characterized for Sr, Nd, and Pb isotopes, and Nb and Zr concentrations, but the available data are quite similar to the enriched 2021 Fagradalsfjall lavas (see bolded Reykjanes Peninsula samples in Figures 10a, 10c, and 10d). These two lavas are subglacial units from Fagradalsfjall (the tuya adjacent to the eruption site) and Lambafell (a hyaloclastite hill in the eastern Reykjanes Peninsula). The similar highly enriched geochemical signatures of the 2021 Fagradalsfjall lavas and certain older lavas on the Reykjanes Peninsula suggests 2021 Fagradalsfjall lavas are not entirely compositionally unique.

Although the 2021 Fagradalsfjall lavas have highly enriched compositions, their Hf-Nd budget is substantially derived from depleted mantle domains. Their signature of high $^{176}Hf/^{177}Hf$ at a given $^{143}Nd/^{144}Nd$ occurs when a depleted melt with high-Hf/Nd, $^{176}Hf/^{177}Hf$, and $^{143}Nd/^{144}Nd$ is mixed with more enriched lower-Hf/Nd melt.

The geochemical effect of mixing the depleted melt into the enriched melt is to increase $^{176}Hf/^{177}Hf$ without substantially changing $^{143}Nd/^{144}Nd$ (see Béguelin et al., 2019; Ferrando et al., 2024; Salters et al., 2011; Sanfilippo et al., 2021; Sani et al., 2023; Stracke et al., 2011). We further note that the geochemical changes are not consistent with the significant addition of pyroxenite melt (Stow et al., 2023). Therefore, a significant quantity of the parental melt of the 2021 Fagradalsfjall lava, as measured by its Hf-Nd budget, is sourced from depleted mantle domains.

The origin of the unusual geochemical composition of the 2021 Fagradalsfjall lava is therefore explained by a superimposition of enriched and depleted geochemical signatures within a single lava chemistry. However, this is not because of simple mixing between melts derived from homogenous depleted and enriched mantle domains. All erupted basalt lavas are formed through a process of *melt aggregation*- the stochastic mixing of near-primary polybaric melts sourced from the heterogeneous mantle domains within the underlying melting region (Maclennan, 2008a, 2008b; Stracke, 2021; Stracke & Bourdon, 2009). The immense compositional diversity of near-primary mantle melts contributing to the erupted lavas of the Reykjanes Peninsula is also reflected in the compositions of melt inclusions. Halldórsson et al. (2022) and Maclennan (2008b) both measured Reykjanes Peninsula melt inclusions and identified a wide range of melt inclusion compositions that encompass the compositions of the 2021 Fagradalsfjall lavas. These include very high Nb/Zr and La/Sm at a given Sm/Yb, similar to the 2021 Fagradalsfjall geochemical signature (Figure 7a). Caracciolo et al. (2023) measured melt inclusions in lavas from the 800–1240 CE Fires and identified a wide range of K_2O/TiO_2 compositions (from ∼0 to 0.5) all along the Reykjanes Peninsula, encompassing the composition of the 2021 Fagradalsfjall lavas. Therefore, in terms of melts supplied from the mantle source as sampled by melt inclusions, the 2021 Fagradalsfjall lava is not compositionally unusual. However, because of its low $^{143}Nd/^{144}Nd$ composition (Figures 7b and 10a), Nb/Zr-Sm/Yb relationships (Figure 7a), and Hf-Nd isotope systematics (Figure 10b) it is distinct from almost all other Icelandic rift basalts except possibly for a few, rare, highly enriched (Figures 10a, 10c, and 10d) and highly depleted (Figure 10b) Reykjanes Peninsula basalts. Erupted basalts differ from melt inclusions in that they have undergone a much greater degree of melt aggregation and homogenization, and their compositions therefore tend to be much less variable than those of melt inclusions. Therefore, the unusual compositions of the 2021 Fagradalsfjall lavas are not the product of typical melt aggregation processes on the Reykjanes Peninsula. We propose that the unusual composition of these basalts is due to a bias in their melt aggregation process that resulted in a larger proportion of compositionally extreme melts, that is, highly depleted and enriched melts, and a lesser proportion of moderately depleted and enriched melts. One example mechanism to create this bias is that some of the mantle melts are "captured" by an adjacent volcanic system. Future work involving quantitative modeling of the melt aggregation process (e.g., Rudge et al., 2013) will reveal the feasibility of this model that, for now, forms a working hypothesis to explain these unusual melt compositions.

6.4. Evidence for the Contribution of Multiple Magma Bodies to the 2021 Fagradalsfjall Eruption

A key feature of the 2021 Fagradalsfjall eruption is that the trace element and radiogenic isotope composition of the lava changes over time. Primitive and deep magma systems contain geochemically heterogeneous magmas, because mixing processes have not yet homogenized them (e.g., Genske et al., 2019; Lambart et al., 2019; Maclennan et al., 2003; Neave, Namur, et al., 2019). One possibility is that the 2021 eruption originates from a single, large, compositionally-zoned magma chamber. However, Maclennan (2019) calculated that a sill containing low-viscosity primitive basalt will homogenize due to convection on a days-to-weeks timescale. This timescale is substantially shorter than the multi-year period of volcanic unrest prior to the 2021 eruption (Kahl et al., 2023), and therefore, given that direct mantle inputs are likely small (see Section 6.2), a more likely explanation of the geochemical variability in the 2021 eruption is that it rather originates from multiple compositionally distinct magma bodies.

Mixing of magma from multiple chemically distinct magma bodies would cause magma compositions to fall along mixing trends. Figure 5 presents several plots that allow for evaluation of the binary mixing process. Macrocryst-free matrix ITE concentrations, ITE ratios, Ni, and MgO concentrations (Figure 5, Figure S7 in Supporting Information S1) fall along binary mixing trends, with scatter along the trends of similar magnitude to analytical uncertainty. These results suggest that the macrocryst-free matrix composition is controlled by mixing of two or more contributing magma bodies, and not by fractional crystallization. Application of melt-based thermometry shows that all erupted compositions have similar calculated temperatures (∼1210°C; Figure S12 in Supporting Information S1; Equations 14–16; Putirka, 2008). Additionally, the apparent adherence to a binary

mixing trend for all measured ITEs, ITE ratios, Ni, and MgO means that processes like fractional crystallization or assimilation must play a limited role (e.g., assimilation fractions less than 0.05) in shaping the geochemical variations of the 2021 Fagradalsfjall carrier melt. For example, significant assimilation would cause lava compositions to fall along an assimilation-fractional crystallization trajectory that would most likely depart from binary mixing trends (DePaolo, 1981). This conclusion is consistent with arguments against significant shallow-level assimilation based on the oxygen isotope compositions of the 2021 Fagradalsfjall lava by Bindeman et al. (2022). Although Day et al. attributed high bulk $^{187}Os/^{188}Os$ and Pt/Ir ratios in the 2021 lava to deep crustal assimilation, we show in Section 6.1 that these features are more likely caused the accumulation of macrocrysts into the carrier melt (See Supporting Information S1).

Radiogenic isotope ratios show that samples do not lie along a single binary mixing trend (Figure 9), despite that radiogenic isotope compositions broadly correlate with ITE concentrations and ratios (Figure S12 in Supporting Information S1). Therefore, the radiogenic isotope compositions of the lavas indicate that more than two magma bodies contributed to the eruption. It is not possible to identify the exact number of magma bodies that supply an eruption through geochemical inference, as different magma bodies may not have distinguishable geochemical compositions. However, it is possible to use geochemical inference to place rough constraints on the minimum number of magma bodies that mix to produce geochemical variability. Given that the concentration ratios of these radiogenic systems (e.g., Hf/Nd, Sr/Nd, Pb/Nd, etc.) have relatively little variation (highest/lowest <1.5) in the 2021 eruption lavas, isotope mixing should generate nearly linear rather than curving trends in isotope space (e.g., Vollmer, 1976). If we assume that each magma body source contains magma of a well-mixed, time-invariant composition, then all geochemical variability in the erupted lavas is related to mixing between magma bodies of different compositions. Given that mixing between magma bodies in the 2021 eruption is not strongly hyperbolic in isotope space, the dimensionality of mixing allows us to place constraints on the number of magma bodies. For example, if sample compositions fell along a line (indicating binary mixing), then it would require, at minimum, two magma bodies to generate that variability, whereas if sample compositions fell along a 2-dimensional plane, then it would take at minimum three magma bodies to explain the variability, and so on.

Principal component analysis (PCA) is a useful tool for identifying the most important vectors of compositional variability within a high-dimensionality data set. Applying PCA to the 2021 Fagradalsfjall lava Sr-Nd-Hf-Pb isotope data results in 98.7% of the variability falling into three principal components, implying that nearly all the observed Sr-Nd-Hf-Pb isotope variability lies within a three-dimensional isotope space (Figure S13 in Supporting Information S1). Therefore, based on the reasoning outlined in the previous paragraph, mixing between a minimum of four magma bodies would be required to explain the isotopic variation in the 2021 Fagradalsfjall lavas. However, this is a minimum estimate, and more contributing magma bodies are likely. Additional magma bodies that contribute significant melt to the eruption may be missed if they have the same magma composition as another body or have a composition that falls along the mixing arrays of the other bodies. For example, the trace element compositions of the 2021 lavas fall along a linear array. In order to reproduce this array, only two endmember magma bodies are required. However, constraints from radiogenic isotopes demand that there are four magma bodies, which shows that all four of the magma bodies contributing to the eruption lie along the linear array defined by trace elements. The observation that the compositions of the different magma bodies all lie along a single mixing array is not a coincidence, and is a direct result of the stochastic melt aggregation processes that accumulate small-volume mantle melts into much larger eruptible volumes (Rudge et al., 2013). Therefore, based on radiogenic isotope compositions, there at least four magma bodies contributing to the eruption, but there are likely more.

What is still not clear is whether these magma bodies interact through recharge of a single, large central magma chamber that supplies the eruption, or whether each small magma body independently supplies the eruptive conduit. If a single large magma chamber supplied the 2021 eruption, the magma composition within a chamber would not experience sudden changes in geochemistry but would instead evolve or wander steadily in composition over time. Although the 2021 Fagradalsfjall lavas do exhibit some steady geochemical change over time, they also exhibit rapid oscillatory changes. For example, sample compositions change from depleted (La/Sm = 1.95) to more enriched (La/Sm = 2.6) and back to more depleted compositions (La/Sm = 2.35) within the first 11 days (the magnitude of the change in these few days is greater than all geochemical variability in the 800–1240 CE fires). Another major oscillation later in the eruption can be seen from days ∼131 to ∼150, where the lava composition has a La/Sm of 3.0 on day ∼131, changing to 2.6 by day ∼140, again to 3.0 on day ∼147, and is then lower to 2.8 on day ∼150. These rapid and oscillatory swings in composition are difficult to reconcile with

recharge events to a large magma chamber and are more consistent with competing rates of magma supply from different magma bodies over time. The rapid compositional changes further show that the eruptive conduit played a limited role in the mixing process, either because of its limited volume, or because the geometry of the conduit prevented efficient mixing.

Together, radiogenic isotope compositions show that multiple (at least four) magma bodies supply magma to the eruption at different times. Over time, the erupted lavas tended to undergo smaller geochemical changes, suggesting that the magmatic system became more stable and less dynamic as the eruption progressed. One interpretation of this is that the eruption was originally fed by many magma bodies, but over time became dominated by fewer bodies with larger volumes as the smaller magma bodies ran out of melt. If so, then the larger magma bodies tended to be enriched, as shown by the progressive changes toward more enriched lava compositions over the course of the eruption. This interpretation that the eruption is fed by many magma bodies is consistent with the notion that deep basalt magmatic systems contain a population of geochemically diverse magmas (e.g., Burton et al., 2024; Genske et al., 2019; Gurenko & Chaussidon, 1995; Lambart et al., 2019; Maclennan, 2008a, 2008b, 2019; Nielsen et al., 1995), however the notion that such a diversity of magmas exist simultaneously in a complex of magma bodies has not been previously shown.

6.5. Influence of Deep Magmatic Processes on Surficial Eruptive Phenomena

Beginning on day 39 of the eruption, there was more than a two-fold increase in the effusion rate of the eruption and the onset of a lava fountaining phase (Figure 6e; Eibl et al., 2023; Pedersen et al., 2022; Scott et al., 2023). This rapid rise in effusion rate after weeks of eruption contrasts sharply with most other Icelandic eruptions, which tend to decline in effusion rate over time due to decreasing magma chamber pressure (Aravena et al., 2020; Pedersen et al., 2022; Wadge, 1981). Critically, this change in eruption style and effusion rate also coincides with a sudden change in the radiogenic isotope composition of the lava (Figure 9). As discussed in Section 6.4, magma compositions in the days prior to eruption day 45 lie along a well-defined trend in terms of radiogenic isotope composition. However, on day ∼45 (i.e., occurring sometime between samples measured for radiogenic isotope compositions on day 41 and 48) there was a sudden shift in the radiogenic isotope composition of the lava (Figures 9a, 9c, and 9d), while the trace element composition stayed relatively constant. We highlight that the compositions of lavas erupted in the period day 39–52 (the interval over which effusion rate changed) only displayed significant change in their isotope ratios, and did not display significant changes in major or trace element composition, temperature, or OPAM equilibration pressure. Consequently, we do not detect any change over this period in the geochemical properties of the lava itself that could influence eruption behavior (e.g., increasing volatile content, viscosity).

Instead, the change in eruptive style, effusion rate, and lava radiogenic isotope composition starting on day 39 could be explained by an increase in magma supply due to recharge. According to Sigmundsson et al. (2020), the driving pressure for upward flow within an eruptive channel is equal to the sum of (a) the buoyancy of the magma at depth, (b) the buoyancy of ascending magma in the eruptive dike, and (c) pressure changes within the magma chamber due to magma recharge. Of these three factors, the first and the second are unlikely to change significantly without a substantial change to the lava composition. However, the third factor, pressure from magma recharge, could explain both the isotopic changes to the erupted lava composition and the change in effusion rate and eruptive style. Given that recharge is occurring, a model for the events surrounding day ∼45 can be conceived: on day 39 (the day of the start of fountaining) an enriched magma body supplying the eruption experiences a significant amount of recharge, shifting its radiogenic isotope composition and increasing the driving pressure in the eruptive conduit. The increase in magma reservoir pressure from this recharge event results in more rapid magma ascent and greater effusion rate. Previous investigation of the connection between magma ascent rate and eruptive style suggests that higher magma ascent rates can push eruption behavior into a Hawaiian-style lava fountaining regime (Parfitt & Wilson, 1995), like that observed in the 2021 eruption. Therefore, deep magma recharge of the magma reservoir can explain the change in isotope composition of the lava, as well as the sudden onset of fountaining and an increase in effusion rate. However, it is possible that the isotopic changes and the change in eruptive behavior are a coincidence, and in this case the onset of fountaining may be instead related to a passing of a behavioral tipping point as the lava becomes steadily more enriched (and therefore more volatile-rich) in the first weeks of the eruption (Figure 6; e.g., Sides et al., 2014).

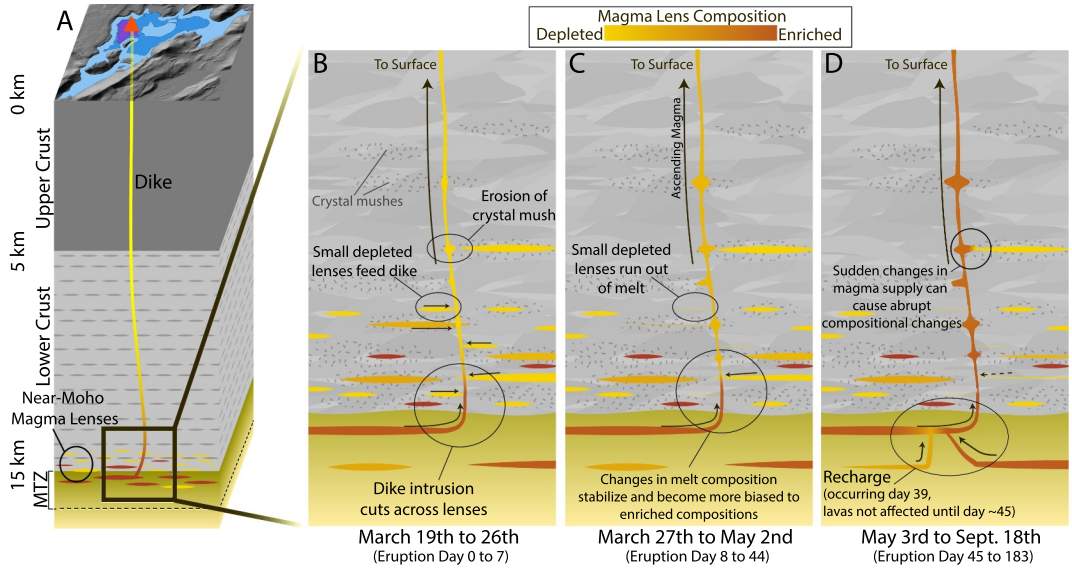

Figure 12. Conceptual diagram of the structure of the 2021 Fagradalsfjall magma plumbing system over the course of the eruption (not to scale). (a) A cross section of the Reykjanes Peninsula crust revealing a complex of melt lenses at the base of the lower crust and within the Moho transition zone. Depths to upper-lower crust transition and crust-mantle transition based on Weir et al. (2001). (b) A dike emanating from an enriched melt lens at the base of the complex propagates upwards, intersecting with multiple small, depleted melt lenses. The contribution of magma from many sills results in a diverse mixture of radiogenic isotope compositions in the early erupted lavas and an overall geochemically depleted composition. (c) From day 8–44, the small depleted sills are exhausted, and the eruption is dominantly supplied by larger enriched sills, with erupted melt compositions becoming increasingly enriched over time. (d) On day 39, the enriched melt lens is recharged by other melt lenses resulting in compositional shifts and an increase in driving pressure of melt into the dike. From this point until the end, the eruption is primarily sourced by large enriched sills; however, sudden changes in the supply network of sills may cause sudden compositional excursions in the erupted lava.

This recharge model can be used to roughly constrain the magma ascent rate of the 2021 Fagradalsfjall eruption. Because the distance from the magma reservoir to the surface is known (~15 km; Weir et al., 2001), we simply need to estimate how long it takes for magma to be transported from the magma reservoir to the surface to be able to calculate an ascent rate. Because pressure travels through a magma-filled dike much more rapidly than magma itself is transported, we predict a delay between the first changes in eruptive style and the first changes in lava chemistry. Assuming that pressure is transmitted through the dike instantaneously, such a delay corresponds to the period of magma transport. The change in isotope composition occurs between days 41 (G20210501-1) and 48 (G20210511-2), corresponding to a delay of 2 (day 39–41) or 9 (day 39–48) days. These delays yield calculated magma ascent rates between 0.02 m/s and 0.09 m/s, which is similar to that determined for Borgarhraun in the Northern Rift Zone (0.02–0.1 m/s; Mutch, Maclennan, Shorttle, et al., 2019).

6.6. A Tentative Model of Events in the Magma Plumbing System of the 2021 Fagradalsfjall Eruption

Geochemical data combined with data from other studies on the 2021 Fagradalsfjall eruption can be used to create a tentative model to serve as a working hypothesis for events occurring beneath Fagradalsfjall leading up to, and during the eruption.

In the years leading up to the 2021 Fagradalsfjall eruption, magma had been accumulating beneath the Reykjanes Peninsula. Between December 2019 and January 2020, seismic swarms and crustal inflation episodes were observed at the Svartsengi and Krýsuvík geothermal fields. These phenomena were attributed to shallow (i.e., 4 km depth) magma injection into the crust and possible magma devolatilization (Cubuk-Sabuncu et al., 2021; Flóvenz et al., 2022). A seismic station network deployed near Fagradalsfjall in June 2020 almost immediately began to detect deep long period seismicity that is associated with magma movement at 10–12 km depth (Greenfield et al., 2022). Diffusion chronometry of olivine and plagioclase macrocrysts in the 2021 Fagradalsfjall lavas find that many olivine diffusion timescales date back to the 2019–2020 period of seismic unrest (Kahl et al., 2023). A few olivine diffusion timescales predate this, suggesting a "priming" phase starting years prior to

the seismic unrest phase. These olivine diffusion timescales show migrating magmas had infiltrated the lowermost crust in the months and years prior to eruption. Geochemical observations presented in this study further suggest that magma accumulation at the near-Moho did not occur in a single large magma chamber, but rather as numerous smaller bodies. Collectively, geophysical, geochemical, and petrological observations point to active magma transport and accumulation both close to the crust-mantle boundary and in the lower crust in the years preceding the eruption.

On 24 February 2021, a dike formed that propagated from the near-Moho up to the upper crust (Figure 12). From thermobarometry constraints (see Section 6.2), the dike likely originated from the lowermost crust or Moho transition zone at the base of a complex of melt lenses in the overlying lowermost lower crust (Section 6.4, Figures 12a and 12b). As the dike propagated upwards, it breached the margins of other melt lenses within the lowermost lower crust, permitting the tapping of compositionally different melt lenses, each having different volumes and compositions. Given that the lava changed very rapidly (on a near-daily basis) in radiogenic isotope composition in the first days of the eruption (days 0–7) and given that these lavas represent the most depleted compositions of the eruption, we posit that the lenses containing the depleted magmas are small and isolated, but numerous. Later in the eruption the lavas became more enriched and the compositional evolution of the eruption stabilized, showing that later the eruption was dominantly supplied by fewer, larger enriched lenses. Furthermore, if the lower OPAM pressures of the early depleted melts is a resolvable feature (see Section 6.2), then the reason that the depleted lavas erupted prior to the enriched lavas is because depleted magmas were more common higher up in the complex of lenses.

The dike propagated to within 1 km of the surface and inflated for 3 weeks prior to the eruption onset (Sigmundsson et al., 2022). During this 3-week period, the dike cooled and began to fractionate. Because stagnant dikes rapidly cool and solidify (a stagnant 1-m-wide dike would crystallize in 3 days; White et al., 2011), all but the thickest portions of the dike would have solidified during this time to form a more pipe-like conduit. The fractionation of the magma at shallower depth in the dike resulted in partial resetting of the dike magma's OPAM barometer to lower pressures. As the dike drew magma from the near-Moho reservoir system to inflate and propagate, it drew magma from the many melt lenses that it cut across (Figure 12b). When the eruption began on 19 March (Day 0) the radiogenic isotope composition of the erupted lava changed rapidly over a week (at rates faster than can be captured by even near-daily sampling) reflecting the compositions of the many small melt lenses sampled by the dike (Day 0–7 compositional group, Section 6.4). As time passed, the smaller lenses became exhausted of magma, leaving a few, larger, enriched, magma lenses remaining to feed the eruption. By day 8, the contribution from small, depleted lenses began to wane, and the eruption began to be increasingly sourced from larger, enriched magma lenses (Section 6.4; Figure 12c).

Until eruption day 39, the K_2O/TiO_2 of the eruption steadily increased, indicating a steadily increasing contribution from the enriched lenses over time, and reached a peak at about day 39 (Figure 6). However, at day 39, one of the enriched lenses feeding the eruption experienced very significant recharge, which caused a shift in the composition of the erupted lava and increased the supply of magma to the eruption (Section 6.5, Figure 12d). On the surface, the increase in magma ascent rate caused the eruption style to change to a new fountaining regime (April 27th, day 39), and increased in effusion rate from ~5.5 m^3/s to ~12 m^3/s (within days ~40–~52; see Section 6.5). Alongside these sudden changes, the lava chemistry underwent a shift in radiogenic isotope composition reflecting the change in composition due to the recharge event (these lavas do not arrive at the surface until days 41–48; See Section 6.5). From day 39 until the end of the eruption, contribution from enriched melt lenses dominated the geochemical composition of the lava (Figure 6). Throughout the eruption, short-duration geochemical excursions to more depleted or enriched compositions were common (Figure 6). Within this model, we explain these excursions to represent the sudden recharge of a magma body, the sudden connection of new magma bodies to the conduit, or perturbations in magma supply caused by erosion of the conduit, or structural collapse of part of the supply network. The final lava flows effused from the vent on 18 September 2021 (day 183).

7. Conclusions

- The major and trace element concentrations, and radiogenic isotope ratios, of 2021 Fagradalsfjall lavas display both gradual and sudden changes over time
- Chemical disequilibrium between macrocrysts and their carrier melt, along with macrocryst textural features, indicate that macrocrysts are disaggregated crystal mushes

- Combined clinopyroxene-melt and OPAM barometry indicate that the magma reservoir system supplying the eruption is located close to the crust-mantle boundary (12–15 km)
- The lava trace element and radiogenic isotope compositional characteristics render the 2021 lavas compositionally distinct from all Icelandic basalts except a few, rare, highly enriched, and highly depleted, Reykjanes Peninsula basalts
- The lavas have unusual Hf-Nd isotopic systematics that indicate magma aggregation from a suite of melts that have a high proportion, relative to most Icelandic basalts, of highly enriched and depleted melts with fewer melts of more moderate composition
- Based on radiogenic isotope systematics, the eruption is sourced from a magma reservoir system containing at least four magma bodies, and likely more
- The changes in effusion rate and eruptive style beginning on day 39 (April 27th) of the eruption is likely the result of the onset of a deep recharge event

The largest geochemical changes in the 2021 Fagradalsfjall eruption were observed in the first 50 days and, as the eruption continued, these lavas were buried. Today, the earliest lavas in the eruption that are still accessible on the surface are from day 22 of the eruption, which, in consultation with Figure 6, shows that all of the most depleted lavas are now buried. Given that the early lavas reflect a substantial proportion of the geochemical variability in the eruption, their absence from this study might result in different conclusions. For example, without those early samples, the study would have likely concluded that fewer magma bodies fed the eruption. However, many of the key findings of this study can be deduced even without those early samples: the mush entrainment process, the unusual enriched composition of the lava, and the eruption source depth. Therefore, comprehensive studies of older basalt units still likely identify many of the same basic observations. However, our study shows very clearly that a single lava unit may not necessarily be homogenous, and can retain high degrees of geochemical variability. Comprehensive sampling of a lava field, particularly lavas that appear to have erupted earlier or later, is essential to sampling as much of an eruption's petrological and geochemical variability as possible.

The 2021 Fagradalsfjall eruption was one of the most well-monitored eruptions ever, where the seismicity, infrasound, ground deformation, gas chemistry, eruptive phenomena, vent effusion rate, lava petrology, and melt geochemistry of the eruption were all continuously monitored. However, these data were controlled by different parts of the volcanic system, and only their sum was able to produce a holistic picture of the Fagradalsfjall system. The seismicity, infrasound, and eruptive phenomena seemed to be controlled by processes in the shallower crust or volcanic edifice (Eibl et al., 2023; Greenfield et al., 2022; Lamb et al., 2022; Scott et al., 2023), whereas the vent effusion rate, deformation, lava petrology and geochemistry were features controlled by processes in the deepest parts of the volcanic system (deformation and effusion rate are closely linked; Lanzi et al., 2024; Pedersen et al., 2022). The volcanic gas geochemistry appeared to be controlled by a combination of shallow and deep processes (Halldórsson et al., 2022; Scott et al., 2023). Clearly, monitoring campaigns that gather a diverse data set do create a substantially fuller picture of a volcanic system. We show that petrological and geochemical monitoring offers a valuable perspective and helps to identify syn-eruptive processes in the deeper parts of the eruptive system.

Volcanic eruptions on the Reykjanes Peninsula have followed the 2021 Fagradalsfjall eruption both within the Fagradalsfjall volcanic system itself and more recently in the adjacent Svartsengi volcanic system, about 6 km away. Given that eruptions occur in ∼1,200-year cycles on the Reykjanes Peninsula, more eruptions should be expected across the peninsula. These first observations of the Reykjanes Peninsula deep magma reservoir system within this new eruptive cycle reveal not a mature and stable magmatic system, but one in a rapidly changing and dynamic state.

Conflict of Interest

The authors declare no conflicts of interest relevant to this study.

Data Availability Statement

Sample details, including sample IGSN identifiers, and all geochemical data used in this manuscript are given in Tables S1–S10 in Supporting Information S2. The data reported here are also contributed to the PetDB (www.earthchem.org/petdb) data repository and additionally available at the EarthChem Library at https://doi.org/10.60520/IEDA/113489.

Acknowledgments
This project was funded by a Icelandic Research Fund grant of excellence 228933-053. Field sampling was supported in part with funds supplied by the Icelandic government. EWM thanks the Icelandic Meteorological Office for maintaining a publicly accessible webcam network throughout the eruption, as it proved essential for making high-quality estimates of lava eruption date, and thanks to Talfan Barnie for showing him how to access it. This paper was improved by thoughtful and constructive reviews by Oliver Higgins and an anonymous reviewer. Thanks to Peter Zeitler for editorial handling and advice that improved the manuscript.

References

Aravena, A., Cioni, R., Coppola, D., de' Michieli Vitturi, M., Neri, A., Pistolesi, M., & Ripepe, M. (2020). Effusion rate evolution during small-volume basaltic eruptions: Insights from numerical modeling. *Journal of Geophysical Research: Solid Earth*, *125*(6), e2019JB019301. https://doi.org/10.1029/2019JB019301

Baker, J., Peate, D., Waight, T., & Meyzen, C. (2004). Pb isotopic analysis of standards and samples using a ^{207}Pb-^{204}Pb double spike and thallium to correct for mass bias with a double-focusing MC-ICP-MS. *Chemical Geology*, *211*(3–4), 275–303. https://doi.org/10.1016/j.chemgeo.2004.06.030

Baxter, R. J. M., Maclennan, J., Neave, D. A., & Thordarson, T. (2023). Depth of magma storage under Iceland controlled by magma fluxes. *Geochemistry, Geophysics, Geosystems*, *24*(7), e2022GC010811. https://doi.org/10.1029/2022GC010811

Béguelin, P., Bizimis, M., McIntosh, E. C., Cousens, B., & Clague, D. A. (2019). Sources vs processes: Unraveling the compositional heterogeneity of rejuvenated-type Hawaiian magmas. *Earth and Planetary Science Letters*, *514*, 119–129. https://doi.org/10.1016/j.epsl.2019.03.011

Bergmanis, E. C., Sinton, J., & Rubin, K. H. (2007). Recent eruptive history and magma reservoir dynamics on the southern East Pacific Rise at 17°30′S. *Geochemistry, Geophysics, Geosystems*, *8*(12), Q12O06. https://doi.org/10.1029/2007GC001742

Bindeman, I., Deegan, F. H., Troll, V. R., Thordarson, T., Höskuldsson, A., Moreland, W., et al. (2022). Diverse mantle components with invariant oxygen isotopes in the 2021 Fagradalsfjall eruption, Iceland. *Nature Communications*, *13*, 1–12. https://doi.org/10.1038/s41467-022-31348-7

Blichert-Toft, J., Chauvel, C., & Albarède, F. (1997). Separation of Hf and Lu for high-precision isotope analysis of rock samples by magnetic sector-multiple collector ICP-MS. *Contributions to Mineralogy and Petrology*, *127*(3), 248–260. https://doi.org/10.1007/s004100050278

Burton, K. W., Parkinson, I. J., & Neave, D. A. (2024). Mantle depletion recorded by olivine and plagioclase megacrysts in oceanic basalts. *Geochemical Perspectives Letters*, *29*, 9–13. https://doi.org/10.7185/geochemlet.2405

Caracciolo, A., Bali, E., Guðfinnsson, G. H., Kahl, M., Halldórsson, S. A., Hartley, M. E., & Gunnarsson, H. (2020). Temporal evolution of magma and crystal mush storage conditions in the Bárðarbunga-Veiðivötn volcanic system, Iceland. *Lithos*, *352–353*, 105234. https://doi.org/10.1016/j.lithos.2019.105234

Caracciolo, A., Bali, E., Halldórsson, S. A., Gudfinnsson, G. H., Kahl, M., Þórðardóttir, I., et al. (2023). Magma plumbing systems and timescale of magmatic processes during historical magmatism on Reykjanes Peninsula. *Earth and Planetary Science Letters*, *621*, 118378. https://doi.org/10.1016/j.epsl.2023.118378

Caracciolo, A., Marshall, E. W., Bali, E., Merill, H. H., Halldórsson, S. A., Matthews, S., et al. (2024). The 2021–23 Fagradalsfjall fires: Geochemical and petrological insights. In *EGU General Assembly 2024, Vienna, Austria*.

Carlson, R. L., & Herrick, C. N. (1990). Densities and porosities in the oceanic crust and their variations with depth and age. *Journal of Geophysical Research*, *95*(B6), 9153–9170. https://doi.org/10.1029/JB095iB06p09153

Cubuk-Sabuncu, Y., Jónsdóttir, K., Caudron, C., Lecocq, T., Parks, M. M., Geirsson, H., & Mordret, A. (2021). Temporal seismic velocity changes during the 2020 rapid inflation at Mt. Þorbjörn-Svartsengi, Iceland, using seismic ambient noise. *Geophysical Research Letters*, *48*(11), e2020GL092265. https://doi.org/10.1029/2020GL092265

Danyushevsky, L. V. (2001). The effect of small amounts of H_2O on crystallisation of mid-ocean ridge and backarc basin magmas. *Journal of Volcanology and Geothermal Research*, *110*(3–4), 265–280. https://doi.org/10.1016/S0377-0273(01)00213-X

Danyushevsky, L. V., & Plechov, P. (2011). Petrolog3: Integrated software for modeling crystallization processes. *Geochemistry, Geophysics, Geosystems*, *12*(7), Q07021. https://doi.org/10.1029/2011GC003516

Day, J. M. D., Kelly, S., Troll, V. R., Moreland, W. M., Cook, G. W., & Thordarson, T. (2024). Deep crustal assimilation during the 2021 Fagradalsfjall Fires, Iceland. *Nature*, *632*(8025), 564–569. https://doi.org/10.1038/s41586-024-07750-0

DePaolo, D. J. (1981). Trace element and isotopic effects of combined wallrock assimilation and fractional crystallization. *Earth and Planetary Science Letters*, *53*(2), 189–202. https://doi.org/10.1016/0012-821X(81)90153-9

Eibl, E. P. S., Thordarson, T., Höskuldsson, Á., Gudnason, E., Dietrich, T., Hersir, G. P., & Ágústsdóttir, T. (2023). Evolving shallow conduit revealed by tremor and vent activity observations during episodic lava fountaining of the 2021 Geldingadalir eruption, Iceland. *Bulletin of Volcanology*, *85*(2), 10. https://doi.org/10.1007/s00445-022-01622-z

Einarsson, P., Eyjólfsson, V., & Hjartardóttir, Á. R. (2023). Tectonic framework and fault structures in the Fagradalsfjall segment of the Reykjanes Peninsula Oblique Rift, Iceland. *Bulletin of Volcanology*, *85*(2), 1–17. https://doi.org/10.1007/s00445-022-01624-x

Ferrando, C., Borghini, G., Sani, C., Genske, F., Ligi, M., Stracke, A., & Sanfilippo, A. (2024). Deep segregation and crystallization of ultra-depleted melts in the sub-ridge mantle. *Chemical Geology*, *644*, 121840. https://doi.org/10.1016/j.chemgeo.2023.121840

Flóvenz, Ó. G., Wang, R., Hersir, G. P., Dahm, T., Hainzl, S., Vassileva, M., et al. (2022). Cyclical geothermal unrest as a precursor to Iceland's 2021 Fagradalsfjall eruption. *Nature Geoscience*, *15*(5), 397–404. https://doi.org/10.1038/s41561-022-00930-5

Genske, F., Stracke, A., Berndt, J., & Klemme, S. (2019). Process-related isotope variability in oceanic basalts revealed by high-precision Sr isotope ratios in olivine-hosted melt inclusions. *Chemical Geology*, *524*, 1–10. https://doi.org/10.1016/j.chemgeo.2019.04.031

Greenfield, T., Winder, T., Rawlinson, N., Maclennan, J., White, R. S., Ágústsdóttir, T., et al. (2022). Deep long period seismicity preceding and during the 2021 Fagradalsfjall eruption, Iceland. *Bulletin of Volcanology*, *84*(12), 101. https://doi.org/10.1007/s00445-022-01603-2

Gudmundsson, M. T., Jónsdóttir, K., Hooper, A., Holohan, E. P., Halldórsson, S. A., Ófeigsson, B. G., et al. (2016). Gradual caldera collapse at Bárdarbunga volcano, Iceland, regulated by lateral magma outflow. *Science*, *353*(6296), aaf8988. https://doi.org/10.1126/science.aaf8988

Gunnarson, S. R., Belart, J. M. C., Óskarsson, B. V., Gudmundsson, M. T., Högnadóttir, T., Pedersen, G. B. M., et al. (2023). Automated processing of aerial imagery for geohazards monitoring: Results from Fagradalsfjall eruption, SW Iceland, August 2022. *Zenodo*. https://doi.org/10.5281/zenodo.7871187

Gurenko, A. A., & Chaussidon, M. (1995). Enriched and depleted primitive melts included in olivine from Icelandic tholeiites: Origin by continuous melting of a single mantle column. *Geochimica et Cosmochimica Acta*, *59*(14), 2905–2917. https://doi.org/10.1016/0016-7037(95)00184-0

Halldórsson, S. A., Bali, E., Hartley, M. E., Neave, D. A., Peate, D. W., Guðfinnsson, G. H., et al. (2018). Petrology and geochemistry of the 2014–2015 Holuhraun eruption, central Iceland: Compositional and mineralogical characteristics, temporal variability and magma storage. *Contributions to Mineralogy and Petrology*, *173*(8), 1–25. https://doi.org/10.1007/s00410-018-1487-9

Halldórsson, S. A., Marshall, E. W., Caracciolo, A., Matthews, S., Bali, E., Rasmussen, M. B., et al. (2022). Rapid shifting of a deep magmatic source at Fagradalsfjall volcano, Iceland. *Nature*, *609*(7927), 529–534. https://doi.org/10.1038/s41586-022-04981-x

Harðardóttir, S., Matthews, S., Halldórsson, S. A., & Jackson, M. G. (2022). Spatial distribution and geochemical characterization of Icelandic mantle end-members: Implications for plume geometry and melting processes. *Chemical Geology*, *604*, 120930. https://doi.org/10.1016/j.chemgeo.2022.120930

Heinonen, J. S., Spera, F. J., & Bohrson, W. A. (2022). Thermodynamic limits for assimilation of silicate crust in primitive magmas. *Geology*, *50*(1), 81–85. https://doi.org/10.1130/G49139.1

Higgins, O., & Stock, M. J. (2024). A new calibration of the OPAM thermobarometer for anhydrous and hydrous mafic systems. *Journal of Petrology*, *65*(5), egae043. https://doi.org/10.1093/petrology/egae043

Kahl, M., Mutch, E. J. F., Maclennan, J., Morgan, D. J., Couperthwaite, F., Bali, E., et al. (2023). Deep magma mobilization years before the 2021 CE Fagradalsfjall eruption, Iceland. *Geology*, *51*(2), 184–188. https://doi.org/10.1130/G50340.1

Kamber, B. S., & Gladu, A. H. (2009). Comparison of Pb purification by anion-exchange resin methods and assessment of long-term reproducibility of Th/U/Pb ratio measurements by quadrupole ICP-MS. *Geostandards and Geoanalytical Research*, *33*(2), 169–181. https://doi.org/10.1111/j.1751-908X.2009.00911.x

Kelemen, P. B., & Aharonov, E. (1998). Periodic formation of magma fractures and generation of layered gabbros in the lower crust beneath oceanic spreading ridges. *Geophysical Monograph Series*, *106*, 267–289. https://doi.org/10.1029/GM106p0267

Kelemen, P. B., Koga, K., & Shimizu, N. (1997). Geochemistry of gabbro sills in the crust-mantle transition zone of the Oman ophiolite: Implications for the origin of the oceanic lower crust. *Earth and Planetary Science Letters*, *146*(3–4), 475–488. https://doi.org/10.1016/s0012-821x(96)00235-x

Koga, K. T., Kelemen, P. B., & Shimizu, N. (2001). Petrogenesis of the crust-mantle transition zone and the origin of lower crustal wehrlite in the Oman ophiolite. *Geochemistry, Geophysics, Geosystems*, *2*(9), 1038. https://doi.org/10.1029/2000GC000132

Korenaga, J., & Kelemen, P. B. (1997). Origin of gabbro sills in the Moho transition zone of the Oman ophiolite: Implications for magma transport in the oceanic lower crust. *Journal of Geophysical Research*, *102*(B12), 27729–27749. https://doi.org/10.1029/97jb02604

Lamb, O. D., Gestrich, J. E., Barnie, T. D., Jónsdóttir, K., Ducrocq, C., Shore, M. J., et al. (2022). Acoustic observations of lava fountain activity during the 2021 Fagradalsfjall eruption, Iceland. *Bulletin of Volcanology*, *84*(11), 96. https://doi.org/10.1007/s00445-022-01602-3

Lambart, S., Koornneef, J. M., Millet, M.-A., Davies, G. R., Cook, M., & Lissenberg, C. J. (2019). Highly heterogeneous depleted mantle recorded in the lower oceanic crust. *Nature Geoscience*, *12*(6), 482–486. https://doi.org/10.1038/s41561-019-0368-9

Lanzi, C., Geirsson, H., Sigmundsson, F., Parks, M. M., & Drouin, V. (2024). Co-eruptive crustal deformation changes associated with the 2021 Fagradalsfjall eruption (SW-Iceland). In *EGU General Assembly 2024*. https://doi.org/10.5194/egusphere-egu24-16352

La Rosa, A., Pagli, C., Wang, H., Sigmundsson, F., Pinel, V., & Keir, D. (2024). Simultaneous rift-scale inflation of a deep crustal sill network in Afar, East Africa. *Nature Communications*, *15*(1), 4287. https://doi.org/10.1038/s41467-024-47136-4

Maclennan, J. (2008a). Concurrent mixing and cooling of melts under Iceland. *Journal of Petrology*, *49*(11), 1931–1953. https://doi.org/10.1093/petrology/egn052

Maclennan, J. (2008b). Lead isotope variability in olivine-hosted melt inclusions from Iceland. *Geochimica et Cosmochimica Acta*, *72*(16), 4159–4176. https://doi.org/10.1016/j.gca.2008.05.034

Maclennan, J. (2019). Mafic tiers and transient mushes: Evidence from Iceland. *Philosophical Transactions of the Royal Society A*, *377*(2139), 20180021. https://doi.org/10.1098/rsta.2018.0021

Maclennan, J., McKenzie, D., Grönvold, K., Shimizu, N., Eiler, J. M., & Kitchen, N. (2003). Melt mixing and crystallization under Theistareykir, northeast Iceland. *Geochemistry, Geophysics, Geosystems*, *4*(11), 8624. https://doi.org/10.1029/2003GC000558

Matthews, S. W., Caracciolo, A., Bali, E., Halldórsson, S., Sigmarsson, O., Guðfinnsson, G., et al. (2024). A dynamic mid-crustal magma domain revealed by the 2023 to 2024 Sundhnúksgígar eruptions, Iceland. *Science*, eadp8778. https://doi.org/10.1126/science.adp8778

Münker, C., Weyer, S., Scherer, E., & Mezger, K. (2001). Separation of high field strength elements (Nb, Ta, Zr, Hf) and Lu from rock samples for MC-ICPMS measurements. *Geochemistry, Geophysics, Geosystems*, *2*(12), 1064. https://doi.org/10.1029/2001GC000183

Mutch, E. J. F., Maclennan, J., Shorttle, O., Edmonds, M., & Rudge, J. F. (2019). Rapid transcrustal magma movement under Iceland. *Nature Geoscience*, *12*(7), 569–574. https://doi.org/10.1038/s41561-019-0376-9

Mutch, E. J. F. F., Maclennan, J., Holland, T. J. B. B., & Buisman, I. (2019). Millennial storage of near-Moho magma. *Science*, *365*(6450), 260–264. https://doi.org/10.1126/science.aax4092

Neave, D. A., Bali, E., Guðfinnsson, G. H., Halldórsson, S. A., Kahl, M., Schmidt, A. S., & Holtz, F. (2019). Clinopyroxene-liquid equilibria and geothermobarometry in natural and experimental tholeiites: The 2014–2015 Holuhraun eruption, Iceland. *Journal of Petrology*, *60*(8), 1653–1680. https://doi.org/10.1093/petrology/egz042

Neave, D. A., & Namur, O. (2022). Plagioclase archives of depleted melts in the oceanic crust. *Geology*, *50*(7), 848–852. https://doi.org/10.1130/G49840.1

Neave, D. A., Namur, O., Shorttle, O., & Holtz, F. (2019). Magmatic evolution biases basaltic records of mantle chemistry towards melts from recycled sources. *Earth and Planetary Science Letters*, *520*, 199–211. https://doi.org/10.1016/j.epsl.2019.06.003

Neave, D. A., & Putirka, K. D. (2017). A new clinopyroxene-liquid barometer, and implications for magma storage pressures under Icelandic rift zones. *American Mineralogist*, *102*(4), 777–794. https://doi.org/10.2138/am-2017-5968

Nicklas, R. W., Brandon, A. D., Waight, T. E., Puchtel, I. S., & Day, J. M. D. (2021). High-precision Pb and Hf isotope and highly siderophile element abundance systematics of high-MgO Icelandic lavas. *Chemical Geology*, *582*, 120436. https://doi.org/10.1016/j.chemgeo.2021.120436

Nielsen, R. L., Crum, J., Bourgeois, R., Hascall, K., Forsythe, L. M., Fisk, M. R., & Christie, D. M. (1995). Melt inclusions in high-An plagioclase from the Gorda Ridge: An example of the local diversity of MORB parent magmas. *Contributions to Mineralogy and Petrology*, *122*(1–2), 34–50. https://doi.org/10.1007/s004100050111

Pallister, J. S., & Hopson, C. A. (1981). Samail ophiolite plutonic suite: Field relations, phase variation, cryptic variation and layering, and a model of a spreading ridge magma chamber. *Journal of Geophysical Research*, *86*(B4), 2593–2644. https://doi.org/10.1029/JB086iB04p02593

Parfitt, E. A., & Wilson, L. (1995). Explosive volcanic eruptions—IX. The transition between Hawaiian-style lava fountaining and Strombolian explosive activity. *Geophysical Journal International*, *121*(1), 226–232. https://doi.org/10.1111/j.1365-246X.1995.tb03523.x

Peate, D. W., Baker, J. A., Jakobsson, S. P., Waight, T. E., Kent, A. J. R., Grassineau, N. V., & Skovgaard, A. C. (2009). Historic magmatism on the Reykjanes Peninsula, Iceland: A snap-shot of melt generation at a ridge segment. *Contributions to Mineralogy and Petrology*, *157*(3), 359–382. https://doi.org/10.1007/s00410-008-0339-4

Pedersen, G. B. M., Belart, J. M. C., Óskarsson, B. V., Gudmundsson, M. T., Gies, N., Högnadóttir, T., et al. (2022). Volume, effusion rate, and lava transport during the 2021 Fagradalsfjall eruption: Results from near real-time photogrammetric monitoring. *Geophysical Research Letters*, *49*(13), e2021GL097125. https://doi.org/10.1029/2021gl097125

Putirka, K. D. (2008). Thermometers and barometers for volcanic systems. *Reviews in Mineralogy and Geochemistry*, *69*(1), 61–120. https://doi.org/10.2138/rmg.2008.69.3

Roeder, P. L., & Emslie, R. F. (1970). Olivine-liquid equilibrium. *Contributions to Mineralogy and Petrology*, *29*(4), 275–289. https://doi.org/10.1007/BF00371276

Rooyakkers, S. M., Carroll, K. J., Gutai, A. F., Winpenny, B., Bali, E., Guðfinnsson, G. H., et al. (2024). Hydraulically linked reservoirs simultaneously fed the 1975–1984 Krafla Fires eruptions: Insights from petrochemistry. *Earth and Planetary Science Letters*, *646*, 118960. https://doi.org/10.1016/j.epsl.2024.118960

Rudge, J. F., Maclennan, J., & Stracke, A. (2013). The geochemical consequences of mixing melts from a heterogeneous mantle. *Geochimica et Cosmochimica Acta*, *114*, 112–143. https://doi.org/10.1016/j.gca.2013.03.042

Salters, V. J. M., Mallick, S., Hart, S. R., Langmuir, C. E., & Stracke, A. (2011). Domains of depleted mantle: New evidence from hafnium and neodymium isotopes. *Geochemistry, Geophysics, Geosystems*, *12*(8), Q08001. https://doi.org/10.1029/2011GC003617

Sæmundsson, K., & Sigurgeirsson, M. (2013). Reykjanes Peninsula. In B. Bessason, F. Sigmundsson, & J. Solnes (Eds.), *Náttúruvá á Íslandi* (pp. 379–401).

Sæmundsson, K., Sigurgeirsson, M., & Friðleifsson, G. Ó. (2020). Geology and structure of the Reykjanes volcanic system, Iceland. *Journal of Volcanology and Geothermal Research*, *391*, 106501. https://doi.org/10.1016/j.jvolgeores.2018.11.022

Sæmundsson, K., Sigurgeirsson, M., Hjartarson, A., Kaldal, I., Kristinsson, S., & Vikingsson, S. (2016). *Geological Map of Southwest Iceland. 1: 100000* (2nd ed.). Iceland geosurvey.

Sanfilippo, A., Salters, V. J. M., Sokolov, S. Y., Peyve, A. A., & Stracke, A. (2021). Ancient refractory asthenosphere revealed by mantle re-melting at the Arctic Mid Atlantic Ridge. *Earth and Planetary Science Letters*, *566*, 116981. https://doi.org/10.1016/j.epsl.2021.116981

Sani, C., Sanfilippo, A., Peyve, A. A., Genske, F., & Stracke, A. (2023). Earth mantle's isotopic record of progressive chemical depletion. *AGU Advances*, *4*(2), 1–18. https://doi.org/10.1029/2022AV000792

Sani, C., Sanfilippo, A., Skolotnev, S., Ligi, M., Genske, F., & Stracke, A. (2024). Sampling Earth's mantle at intra-transform spreading ridges. *Geochimica et Cosmochimica Acta*, *374*, 156–172. https://doi.org/10.1016/j.gca.2024.04.032

Scott, S., Pfeffer, M., Oppenheimer, C., Bali, E., Lamb, O. D., Barnie, T., et al. (2023). Near-surface magma flow instability drives cyclic lava fountaining at Fagradalsfjall, Iceland. *Nature Communications*, *14*(1), 6810. https://doi.org/10.1038/s41467-023-42569-9

Sides, I. R., Edmonds, M., Maclennan, J., Swanson, D. A., & Houghton, B. F. (2014). Eruption style at Kilauea Volcano in Hawai'i linked to primary melt composition. *Nature Geoscience*, *7*(6), 464–469. https://doi.org/10.1038/ngeo2140

Sigmarsson, O., Condomines, M., Grönvold, K., & Thordarson, T. (1991). Extreme magma homogeneity in the 1783–84 Lakagigar Eruption: Origin of a large volume of evolved basalt in Iceland. *Geophysical Research Letters*, *18*(12), 2229–2232. https://doi.org/10.1029/91GL02328

Sigmundsson, F., Parks, M., Hooper, A., Geirsson, H., Vogfjörd, K. S., Drouin, V., et al. (2022). Deformation and seismicity decline before the 2021 Fagradalsfjall eruption. *Nature*, *609*(7927), 523–528. https://doi.org/10.1038/s41586-022-05083-4

Sigmundsson, F., Pinel, V., Grapenthin, R., Hooper, A., Halldórsson, S. A., Einarsson, P., et al. (2020). Unexpected large eruptions from buoyant magma bodies within viscoelastic crust. *Nature Communications*, *11*(1), 2403. https://doi.org/10.1038/s41467-020-16054-6

Stokes, G. G. (1856). On the effect of the internal friction of fluids on the motion of pendulums. *Transactions of the Cambridge Philosophical Society*, *9*, 8–106.

Stow, M. A., Prytulak, J., Burton, K. W., Nowell, G. M., Marshall, E. W., Halldórsson, S. A., et al. (2023). No V-Fe-Zn isotopic variation in basalts from the 2021 Fagradalsfjall eruption. *Geochemical Perspectives Letters*, *27*, 54–58. https://doi.org/10.7185/geochemlet.2335

Stracke, A. (2021). A process-oriented approach to mantle geochemistry. *Chemical Geology*, *579*, 120350. https://doi.org/10.1016/j.chemgeo.2021.120350

Stracke, A., & Bourdon, B. (2009). The importance of melt extraction for tracing mantle heterogeneity. *Geochimica et Cosmochimica Acta*, *73*(1), 218–238. https://doi.org/10.1016/j.gca.2008.10.015

Stracke, A., Snow, J. E., Hellebrand, E., von der Handt, A., Bourdon, B., Birbaum, K., & Günther, D. (2011). Abyssal peridotite Hf isotopes identify extreme mantle depletion. *Earth and Planetary Science Letters*, *308*(3–4), 359–368. https://doi.org/10.1016/j.epsl.2011.06.012

Thirlwall, M. F., Gee, M. A. M., Taylor, R. N., & Murton, B. J. (2004). Mantle components in Iceland and adjacent ridges investigated using double-spike Pb isotope ratios. *Geochimica et Cosmochimica Acta*, *68*(2), 361–386. https://doi.org/10.1016/S0016-7037(03)00424-1

Todd, E., Stracke, A., & Scherer, E. E. (2015). Effects of simple acid leaching of crushed and powdered geological materials on high-precision Pb isotope analyses. *Geochemistry, Geophysics, Geosystems*, *16*(7), 2276–2302. https://doi.org/10.1002/2015GC005804

Townsend, M., & Huang, M. H. (2022). Timescales of dike growth and chamber deflation constrain magma storage and transport pathways during Kīlauea's 2018 lower East Rift Zone intrusion. *Journal of Geophysical Research: Solid Earth*, *127*(12), e2022JB025636. https://doi.org/10.1029/2022JB025636

Ustunisik, G. K., Nielsen, R. L., & Walker, D. (2021). The missing magmas of MOR: Insights from phase equilibrium experiments on plagioclase ultraphyric basalts. *Geochemistry, Geophysics, Geosystems*, *23*(1), e2021GC009943. https://doi.org/10.1029/2021gc009943

Vollmer, R. (1976). Rb-Sr and U-Th-Pb systematics of alkaline rocks: The alkaline rocks from Italy. *Geochimica et Cosmochimica Acta*, *40*(3), 283–295. https://doi.org/10.1016/0016-7037(76)90205-2

Wadge, G. (1981). The variation of magma discharge during basaltic eruptions. *Journal of Volcanology and Geothermal Research*, *11*(2–4), 139–168. https://doi.org/10.1016/0377-0273(81)90020-2

Weir, N. R. W., White, R. S., Brandsdóttir, B., Einarsson, P., Shimamura, H., & Shiobara, H. (2001). Crustal structure of the northern Reykjanes Ridge and Reykjanes Peninsula, southwest Iceland. *Journal of Geophysical Research*, *106*(B4), 6347–6368. https://doi.org/10.1029/2000jb900358

Weis, D., Kieffer, B., Hanano, D., Silva, I. N., Barling, J., Pretorius, W., et al. (2007). Hf isotope compositions of U.S. Geological survey reference materials. *Geochemistry, Geophysics, Geosystems*, *8*(6), Q06006. https://doi.org/10.1029/2006GC001473

Weis, D., Kieffer, B., Maerschalk, C., Barling, J., De Jong, J., Williams, G. A., et al. (2006). High-precision isotopic characterization of USGS reference materials by TIMS and MC-ICP-MS. *Geochemistry, Geophysics, Geosystems*, *7*(8), Q08006. https://doi.org/10.1029/2006GC001283

Wenrich, W., Bali, E., Marshall, E. W., & Guðfinnsson, G. H. (2022). Origin of gabbro and anorthosite mineral clusters in Fagradalsfjall lavas. In *EGU General Assembly 2022*.

White, R. S., Drew, J., Martens, H. R., Key, J., Soosalu, H., & Jakobsdóttir, S. S. (2011). Dynamics of dyke intrusion in the mid-crust of Iceland. *Earth and Planetary Science Letters*, *304*(3–4), 300–312. https://doi.org/10.1016/j.epsl.2011.02.038

Wieser, P. E., Petrelli, M., Lubbers, J., Wieser, E., Özaydın, S., Kent, A. J. R., & Till, C. B. (2022). Thermobar: An open-source Python3 tool for thermobarometry and hygrometry. *Volcanica*, *5*(2), 349–384. https://doi.org/10.30909/vol.05.02.349384

References From the Supporting Information

Barnes, S. J., Mungall, J. E., & Maier, W. D. (2015). Platinum group elements in mantle melts and mantle samples. *Lithos*, *232*, 395–417. https://doi.org/10.1016/j.lithos.2015.07.007

Bohrson, W. A., & Spera, F. J. (2001). Energy-constrained open-system magmatic processes II: Application of energy-constrained assimilation–fractional crystallization (EC-AFC) model to magmatic systems. *Journal of Petrology*, *42*, 1019–1041.

Maclennan, J., McKenzie, D., Hilton, F., Gronvöld, K., & Shimizu, N. (2003). Geochemical variability in a single flow from northern Iceland. *Journal of Geophysical Research*, *108*(B1). ECV 4-1–ECV 4-21. https://doi.org/10.1029/2000JB000142

Michael, P. (1995). Regionally distinctive sources of depleted MORB: Evidence from trace elements and H_2O. *Earth and Planetary Science Letters*, *131*(3–4), 301–320. https://doi.org/10.1016/0012-821X(95)00023-6